

## RESEARCH ARTICLE

# APOE $\epsilon$ 4-associated heterogeneity of neuroimaging biomarkers across the Alzheimer's disease continuum

Jason Mares<sup>1,2</sup> | Gautam Kumar<sup>1,3,4</sup> | Anurag Sharma<sup>1,3</sup> | Sheina Emrani<sup>5</sup> |  
Laura Beth McIntire<sup>6</sup> | Jia Guo<sup>7,8</sup> | Vilas Menon<sup>1,2</sup> | Tal Nuriel<sup>1,3</sup>  | for the  
Alzheimer's Disease Neuroimaging Initiative

<sup>1</sup>Taub Institute for Research on Alzheimer's Disease and the Aging Brain, Columbia University, New York, New York, USA

<sup>2</sup>Department of Neurology, Columbia University, New York, New York, USA

<sup>3</sup>Department of Pathology and Cell Biology, Columbia University, New York, New York, USA

<sup>4</sup>Department of Neurobiology, University of Maryland, Baltimore, Maryland, USA

<sup>5</sup>Department of Neurology, Perelman School of Medicine, University of Pennsylvania, Philadelphia, Pennsylvania, USA

<sup>6</sup>Lipidomics and Biomarker Discovery Lab, Brain Health Imaging Institute, Department of Radiology, Weill Cornell Medicine, New York, New York, USA

<sup>7</sup>Department of Psychiatry, Columbia University, New York, New York, USA

<sup>8</sup>Zuckerman Institute, Columbia University, New York, New York, USA

## Correspondence

Tal Nuriel, Taub Institute for Research on Alzheimer's Disease and the Aging Brain, Columbia University, 630 W. 168th St., P&S 12-420E, New York, NY 10032, USA.  
Email: [tn2283@cumc.columbia.edu](mailto:tn2283@cumc.columbia.edu)

The Alzheimer's Disease Neuroimaging Initiative: Data used in preparation of this article were obtained from the Alzheimer's Disease Neuroimaging Initiative (ADNI) database ([adni.loni.usc.edu](http://adni.loni.usc.edu)). As such, the investigators within the ADNI contributed to the design and implementation of ADNI and/or provided data, but did not participate in analysis or writing of this report.

## Funding information

NIA, Grant/Award Numbers: K01 AG061264, R01 AG070202, R01 AG078800, R01 AG066831, U19 AG024904

## Abstract

**INTRODUCTION:** While the role of apolipoprotein E (APOE)  $\epsilon$ 4 in Alzheimer's disease (AD) susceptibility has been studied extensively, much less is known about the differences in disease presentation in APOE  $\epsilon$ 4 carriers versus non-carriers.

**METHODS:** To help elucidate these differences, we performed a broad analysis comparing the regional levels of six different neuroimaging biomarkers in the brains of APOE  $\epsilon$ 4 carriers versus non-carriers who participated in the Alzheimer's Disease Neuroimaging Initiative (ADNI).

**RESULTS:** We observed significant APOE  $\epsilon$ 4-associated heterogeneity in regional amyloid beta deposition, tau accumulation, glucose uptake, brain volume, cerebral blood flow, and white matter hyperintensities within each AD diagnostic group. We also observed important APOE  $\epsilon$ 4-associated differences in cognitively unimpaired individuals who converted to mild cognitive impairment/AD versus those who did not convert.

**DISCUSSION:** This observed heterogeneity in neuroimaging biomarkers between APOE  $\epsilon$ 4 carriers versus non-carriers may have important implications regarding the prevention, diagnosis, and treatment of AD in different subpopulations.

## KEYWORDS

Alzheimer's disease, Alzheimer's Disease Neuroimaging Initiative, apolipoprotein E, biomarkers, heterogeneity, neuroimaging

This is an open access article under the terms of the [Creative Commons Attribution-NonCommercial](https://creativecommons.org/licenses/by-nc/4.0/) License, which permits use, distribution and reproduction in any medium, provided the original work is properly cited and is not used for commercial purposes.

© 2025 The Author(s). *Alzheimer's & Dementia* published by Wiley Periodicals LLC on behalf of Alzheimer's Association.

### Highlights

- An extensive study was performed on the apolipoprotein E (APOE)  $\epsilon 4$ -associated heterogeneity in neuroimaging biomarkers from the Alzheimer's Disease Neuroimaging Initiative.
- Robust APOE  $\epsilon 4$ -associated increases in amyloid beta ( $A\beta$ ) deposition throughout the brain, in every diagnostic group, were observed.
- APOE  $\epsilon 4$ -associated increases in tau pathology, decreases in glucose uptake, and increases in brain atrophy, which expand in regional scope and magnitude with disease progression, were observed.
- Significant sex- and age-related differences in APOE  $\epsilon 4$ -associated neuroimaging biomarker heterogeneity, with overall increases in pathological presentation in female APOE  $\epsilon 4$  carriers, were observed.
- Regional differences in  $A\beta$  deposition, tau accumulation, glucose uptake, ventricle size, and white matter hyperintensities were observed in cognitively normal participants who converted to mild cognitive impairment/Alzheimer's disease, which may hold potential predictive value.

## 1 | BACKGROUND

Possession of the apolipoprotein E (APOE)  $\epsilon 4$  allele is the primary genetic risk factor for the late-onset form of Alzheimer's disease (AD). While there have been numerous investigations into the mechanism(s) responsible for this increased risk of AD among APOE  $\epsilon 4$  carriers, far less research has been performed to understand the specific differences in AD-related pathology that occur in the brains of APOE  $\epsilon 4$  carriers versus non-carriers. This information is critical, however, as we enter a new era of AD research and treatment, in which different subpopulations of patients and at-risk individuals may require different approaches for preventing, diagnosing, and treating the disease.

Fortunately, large cohort studies on human subjects have provided AD researchers with significant amounts of publicly available data, which can be utilized to interrogate the APOE  $\epsilon 4$ -associated differences in AD development and presentation. One such cohort is the Alzheimer's Disease Neuroimaging Initiative (ADNI), which has been collecting neuroimaging data from elderly individuals (participants range from 55 to 90 years old at the start of the study) for the past two decades. For this study, we used six previously compiled neuroimaging datasets available from ADNI: florbetapir positron emission tomography (PET) measurements of amyloid beta ( $A\beta$ ) deposition, flortaucipir PET measurements of tau accumulation, fluorodeoxyglucose (FDG) PET measurements of glucose uptake, structural magnetic resonance imaging (MRI) measurements of brain volume, arterial spin labeling (ASL) MRI measurements of cerebral blood flow (CBF), and fluid-attenuated inversion recovery (FLAIR) MRI measurements of white matter hyperintensities (WMHs).

Each of these neuroimaging biomarkers represent an important pathological manifestation that has been reported either in mild cognitive impairment (MCI)/AD patients, or in cognitively unimpaired APOE

$\epsilon 4$  carriers prior to the development of AD (or in both). Amyloid and tau are well known as the two primary hallmarks of AD pathology, which were first observed in the brain of Auguste Deter by Dr. Alois Alzheimer in the early 1900s.<sup>1</sup> Structural MRI measurement of brain atrophy/neurodegeneration is now recognized as an equally important biomarker of AD, with the A/T/N classification scheme adding neurodegeneration (N) as an essential component for tracking the pathogenesis of AD, along with  $A\beta$  (A) and tau (T).<sup>2</sup> Decreased glucose uptake, as measured by FDG PET, was also discovered early on as an important phenomenon that occurs in the AD brain, as well as in young/middle-aged APOE  $\epsilon 4$  carriers long before the development of AD;<sup>3-5</sup> in both scenarios, the decreased glucose uptake primarily occurs in regions associated with the default mode network (DMN), which includes the posterior cingulate cortex/precuneus, the medial prefrontal cortex, and the angular gyrus.<sup>6</sup> Dysregulated neuronal excitability is another phenotype that has been reported during early AD pathogenesis and in cognitively unimpaired APOE  $\epsilon 4$  carriers. While this dysregulated excitability has most commonly been reported during task-based blood oxygenation level dependent (BOLD) MRI studies,<sup>7-15</sup> other AD and APOE  $\epsilon 4$  studies have used ASL MRI measurements of resting-state CBF levels (see review by Zhang et al.<sup>16</sup>), which is correlated with brain activity. Finally, numerous investigations have also reported increased detection of WMHs in the brains of AD patients,<sup>17-19</sup> which is generally hypothesized to be an indicator of vascular impairments,<sup>20</sup> although alternative explanations exist as well.<sup>21</sup>

For our analyses, we performed separate comparisons of each neuroimaging biomarker in the brains of APOE  $\epsilon 4$  carriers versus non-carriers. First, we measured the overall differences within each of the three diagnostic groups classified by ADNI (cognitively normal [CN], MCI, and AD), controlling for sex and age between the APOE  $\epsilon 4$  carrier and non-carrier groups. Then, we performed separate analyses strati-

fyng the diagnostic groups specifically by either sex or by age. Lastly, we compared the regional levels of each biomarker in CN individuals who converted to MCI or AD during their participation in ADNI versus CN individuals who did not convert, stratified by their *APOE*  $\epsilon$ 4 carrier status. This broad investigation of the *APOE*  $\epsilon$ 4-associated heterogeneity of neuroimaging biomarkers provides a detailed picture of how possession of the *APOE*  $\epsilon$ 4 allele affects the regional susceptibility to different AD-related pathological manifestations across the AD continuum.

## 2 | METHODS

### 2.1 | Participants/datasets

All neuroimaging data used for this study were downloaded as pre-processed datasets from ADNI ([adni.loni.usc.edu](http://adni.loni.usc.edu)). ADNI was launched in 2003 as a public-private partnership, led by Dr. Michael Weiner. ADNI's primary goal has been to test whether serial MRI, PET, and other biological markers, as well as clinical and neuropsychological assessments, can be combined to measure the progression of MCI and early AD dementia. The specific ADNI datasets used for this study are as follows: (1)  $A\beta$  PET analysis using florbetapir, performed by Dr. Susan Landau, Dr. William Jagust, and colleagues at University of California (UC) Berkeley, which included participants from ADNI1/GO/2/3 (version 2023-06-29); (2) tau PET analysis with partial volume correction (PVC) using flortaucipir, performed by Dr. Susan Landau, Dr. William Jagust, and colleagues at UC Berkeley, which included participants from ADNI2/3 (version 2023-09-27); (3) FDG PET analysis, performed by Dr. Susan Landau, Dr. William Jagust, and colleagues at UC Berkeley, which included participants from ADNI1/GO/2/3 (version 2023-02-17); (4) cross-sectional structural MRI analysis, performed by Dr. Duygu Tosun-Turgut, Dr. Norbert Schuff, Dr. Michael Weiner, and colleagues at UC San Francisco (UCSF), which included participants from ADNI1/GO/2 (version 2019-11-08); (5) ASL MRI CBF analysis, performed by Dr. Duygu Tosun-Turgut, Dr. Norbert Schuff, and colleagues at UCSF, which included participants from ADNI3 (version 2022-08-17); and (6) FLAIR MRI WMH analysis, performed by Dr. Owen Carmichael, Dr. Charles DeCarli, and colleagues at UC Davis, which included participants from ADNI1/GO/2/3 (version 2022-05-02).

### 2.2 | Data processing

We performed the following additional processing for each dataset:

1.  $A\beta$  PET: We considered only data that were obtained using the "FBP" (florbetapir) tracer. Each region of interest (ROI) standardized uptake value ratio (SUVR) value available in the dataset had already been intensity normalized to the whole cerebellum, so no additional normalization was performed.
2. Tau PET: We considered only data that were obtained using the "FTP" (flortaucipir) tracer. The ROI SUVRs in this dataset were

### RESEARCH IN CONTEXT

1. **Systematic review:** The authors reviewed the literature related to changes in any of the six neuroimaging biomarkers studied here in apolipoprotein E (*APOE*)  $\epsilon$ 4 carriers versus non-carriers. A concise summary of the previous research with each of these biomarkers is included in the Introduction.
2. **Interpretation:** While studies have been performed previously using these neuroimaging biomarkers in *APOE*  $\epsilon$ 4 carriers versus non-carriers, these studies were often performed on relatively small cohorts. In addition, we did not observe any published studies that analyzed all six biomarkers at the same time and with the same statistical approaches used in this study.
3. **Future directions:** The comprehensive picture of *APOE*  $\epsilon$ 4-associated heterogeneity in neuroimaging biomarkers that we have presented here provides a powerful framework for future investigations into *APOE*  $\epsilon$ 4 and its role in Alzheimer's disease (AD) pathogenesis, as well as investigations into the inherent differences in disease presentation and pathogenesis between *APOE*  $\epsilon$ 4 carriers and non-carriers. Importantly, this heterogeneity should be taken into consideration during diagnosis, prevention, and therapeutic studies of different subpopulations of AD patients and at-risk individuals.

intensity normalized to the inferior cerebellar gray matter, and no additional normalization was performed.

3. FDG PET: In the updated versions of their analysis, the UC Berkeley investigators combined the FDG PET results from five separate ROIs (left angular gyrus, right angular gyrus, left inferior temporal gyrus, right inferior temporal gyrus, and bilateral posterior cingulate cortex) into one "MetaROI." We further processed the data by intensity normalizing the MetaROI values for each participant to the Top50PonsVermis (mean of the top 50% of the pons/vermis) reference ROI, as per the researchers' instructions. Our analyses only focused on the normalized MetaROI measure for each sample.
4. Structural MRI: For the cross-sectional structural MRI dataset, we only considered samples that passed the OVERALLQC metric. In addition, for ROIs that failed the regional quality control (QC) metric, we set the data pertaining to the given ROI as missing. For downstream analysis, we only used the cortical volume (CV) and subcortical volume (SV) measurements for the ROIs. The data were z score normalized across the entire dataset. All regional analyses with this dataset were also controlled for total intracranial volume, identified in the dataset as the ICV\_CV variable.
5. ASL MRI: For the CBF measurements using ASL MRI, we considered only samples with a PASS in the RAWQC variable. For samples with ROIs that failed QC, we labeled the data in this ROI as missing. For

downstream analysis, we only focused on the average (AVG) measurements for each ROI. The data were z score normalized across the entire dataset.

6. FLAIR MRI: For the WMH measurements using FLAIR MRI, we considered only the "TOTAL\_WMH" measurements, as the other datapoints provided were volumetric measures that are included in our structural MRI analysis. The data were log and then z score normalized across the entire dataset. All regional analyses with this dataset were also controlled for total intracranial volume, identified in the dataset as the CEREBRUM\_TCV variable.

For datasets with multiple features, we omitted individual records that did not have data for at least 20% of the available measurements. We then filtered for measurements with complete data across the remaining records in the dataset. Additional information about each participant was obtained from the ADNIMERGE file downloaded from ADNI.

### 2.3 | Statistical analyses

The two independent variables of interest across our analyses were APOE  $\epsilon$ 4 carrier status or converter status. APOE  $\epsilon$ 4 carrier status was encoded as 0 if the participant carried no APOE  $\epsilon$ 4 alleles, and 1 if they possessed at least one APOE  $\epsilon$ 4 allele. Converter status was encoded as 0 if the participant was diagnosed as CN at the visit and would not be diagnosed with MCI or AD at a later visit, and 1 if they were diagnosed as CN at the visit and their diagnosis changed to MCI or AD at a later visit. For the stratifications, sex was encoded as 0 for female and 1 for male. For our age stratification analysis, we created a binary age variable that encoded 0 if examination visit dates occurred when the participant was < 75 years old and 1 if examination visit dates occurred when the participant was  $\geq$  75 years old. Age was calculated using the age listed during the participant's baseline visit, plus the difference between the date of the baseline visit and the date of the subsequent examination visits listed in each dataset.

Prior to the statistical analyses, the participant trajectories of diagnosis were examined to look for potential irregularities. Irregularities were identified as any unexpected blips in trajectory (e.g., MCI diagnosis followed by a CN diagnosis). There was a total of 148 (of 2088) participants with records showing an unexpected change in diagnosis. From these, 13 contained multiple such reversions, while 135 showed a single incident of reversion; the 13 participants with multiple reversions were removed from our analysis. When examining the remaining 135, we additionally removed 59 participants who either only had two visit records or who showed a long-term endurable change in diagnosis (e.g., reverted from MCI to CN and then remained CN for the remainder of the study). While this latter group is of interest, these participants are likely to have some fundamental differences to the rest of the cohort. For the remaining 76 participants with a single reversion, we included their neuroimaging data in the analysis, but removed the individual visit record of the unexpected change in diagnosis.

In addition, there were cases in which the clinical diagnosis of a participant at a given visit was not available in the metadata; for these participants, we imputed a clinical diagnosis if the following three conditions were met: (1) the participant had at least three records, one of which was the visit with the missing diagnosis, (2) there was a recorded diagnosis for the visits before and after the given visit with the missing diagnosis, and (3) the diagnosis for the two visits before and after the missing diagnosis was concordant. Thus, in these imputed cases, we assumed that clinical diagnosis remained unchanged.

After these adjustments, we analyzed the data using a linear mixed-effects model performed across each of the six biomarker datasets. This analysis was conducted using the lmer command with default settings from the R lmer4 package. All models included sex and age at visit as control variables, except the sex- and age-stratified analyses, which only included one or the other as control variables. For models involving structural MRI and FLAIR MRI, we also controlled for total intracranial volume. Due to the longitudinal nature of the data obtained in ADNI, we opted for a donor-based random-intercept model based on participant clusters. This approach has the benefit of using all available data from the cohort, while also recognizing that longitudinal data from the same participant are correlated and should be not be independent data points.

It should also be noted that some datasets in our stratified models contained a moderate proportion of singletons (one scan/participant); this measure ranged from 9.9% to 54.7% (Table S1 in supporting information). Although the number of singleton clusters is high, it is not unexpected from this type of dataset. Importantly, previous literature suggests that the number of singleton clusters may not lead to serious bias or increased Type 1 errors.<sup>22,23</sup> Instead, statistical power is more impacted by the number of clusters; in our case, the ASL MRI dataset has the smallest number of clusters at 369, while the FDG PET dataset has the largest number at 1553. For each analysis, we corrected for multiple testing using the Benjamini-Hochberg method, apart from the FDG PET and FLAIR MRI analyses, which only focused on one combined ROI in each analysis.

For the machine learning analysis, we used available biomarker data at earliest visits from CN participants (often baseline). We found the greatest overlap of participants to be between the A $\beta$  PET, FDG PET, STRUCTURAL MRI, and FLAIR MRI analyses. Due to the limited number of converters with overlapping data, we restricted the number of features used for this analysis, so as not to risk overfitting the models. The regions/modalities used were: CAUDALANTERIORCINGULATE (A $\beta$  PET), LH\_ROSTRALANTERIORCINGULATE (A $\beta$  PET), LEFT\_ACCUMBENS\_AREA (A $\beta$  PET), SUPERIORFRONTAL (A $\beta$  PET), RightInferiorLateralVentricle\_SV (STRUCTURAL MRI), TOTAL\_WMH (FLAIR MRI), and MetaROI (FDG PET).

For supervised learning of participant converter status, we used the h2o package to fit the data across multiple machine learning algorithms. One of h2o's functions, h2o.automl, was used to randomly fit 40 different models set at random parameters on the data. The balance\_classes parameter was enabled due to the unbalance nature of the dataset. When fitting XGBoosted models, we also set additional hyperparameter values based on random combinations from a value

grid based on number of trees, maximum tree depth, sample rate, learn, and rate hyperparameters. To reduce overfitting, we enabled 3-fold stratified cross-folding validation. We split the dataset into one training set and one test set, dividing each group (*APOE*  $\epsilon$ 4 carrier converters, *APOE*  $\epsilon$ 4 non-carrier converters, *APOE*  $\epsilon$ 4 carrier non-converters, and *APOE*  $\epsilon$ 4 non-carrier non-converters) 60/40 into the training set and the test set. In our analysis, we also considered two subsets of the test set, split by *APOE*  $\epsilon$ 4 carrier status. Finally, from the training set, we fit 50 separate models with randomly selected combination of hyperparameters and evaluated the performance of these models on our training and test sets using the following metrics: area under the curve (AUC), area under the precision recall curve (AUC-PR), and log-loss.

## 2.4 | Brain region/template visualizations

We used 3D Slicer 5.6.2 to create human brain templated visualizations of all significantly different regions (adjusted *p* value < 0.05 for  $A\beta$  PET, tau PET, structural MRI, and ASL MRI; unadjusted *p* value < 0.05 for FDG PET and FLAIR MRI). To accomplish this, we imported the APARC + ASEG segmentation atlas from FreeSurfer and matched the ROIs listed in each of the six datasets with the available ROIs in the FreeSurfer template. Because syntax between datasets and FreeSurfer templates often mismatched, we normalized ROI syntax and, in some cases, prioritized more refined regions over broader types (e.g., breaking down “amygdala” into right and left amygdala).

For each visualization, the axial, coronal, and sagittal axes were adjusted manually to optimize the number of significant features that could be viewed. The brain template was kept at grayscale, while significantly affected ROIs were plotted on a red–white–blue color scale, with the intensity of each ROI color shade corresponding to the magnitude of the statistical difference (beta). Color legends were kept consistent across results from multiple related analyses focused on the same biomarker.

Finally, for the FDG PET and FLAIR MRI WMH visualizations, we chose to use specific ROIs to represent these data, which may not exactly match how the measures were displayed in the actual scans. For FDG PET, we created our own MetaROI group using the left and right posterior cingulate cortex, as well as the left and right inferior parietal cortex (which includes the left and right angular gyrus), and the left and right inferior temporal cortex (which includes the left and right inferior temporal gyrus). For FLAIR MRI WMH results, we used the entire cerebral white matter ROI, because the investigators did not specify where in the white matter their TOTAL\_WMHS were observed.

## 3 | RESULTS

### 3.1 | *APOE* $\epsilon$ 4-associated differences by diagnostic group

As an initial assessment of the *APOE*  $\epsilon$ 4-associated heterogeneity of neuroimaging biomarkers in ADNI participants, we first performed

direct comparisons of the regional biomarker levels revealed by  $A\beta$  PET, tau PET, FDG PET, structural MRI, ASL MRI, and FLAIR MRI measurements in *APOE*  $\epsilon$ 4 carriers versus non-carriers, focusing on the *APOE*  $\epsilon$ 4-associated differences that exist within each diagnostic group (CN, MCI, or AD), as determined by cognitive testing at the time of the participants' scans. For each comparison, *APOE*  $\epsilon$ 4 carrier status was used as the independent variable, and the regional level of each biomarker was used as the dependent variable, with each analysis controlled for sex and age of the participant (further details provided in the Methods section). Importantly, each of these neuroimaging biomarkers were originally scanned in different sets of ADNI participants, so we have provided the numbers and demographic information of the participants from each analysis separately (Table 1).

Comparisons between *APOE*  $\epsilon$ 4 carriers and non-carriers for each diagnostic group were performed using a linear mixed-effects model across each of the six biomarker datasets. Importantly, we chose not to perform any longitudinal analyses (i.e., comparing the rates of biomarker changes over time) because for each of the datasets, a large percentage of the participants only underwent one or two scans for that particular neuroimaging modality (Table S1). Instead, our linear mixed-effects model uses each longitudinal datapoint to increase statistical power and accuracy, with this information summarized into fixed biomarker levels from each diagnostic stage. After our statistical analyses, brain regions with significantly different pathology levels between *APOE*  $\epsilon$ 4 carriers versus non-carriers were graphed onto a box plot, as well as rendered onto a human brain template to help visualize the results, with the color intensity of each region representing the magnitude of the statistical difference (beta).

As displayed in Figure 1A, we observed *APOE*  $\epsilon$ 4-associated increases in regional  $A\beta$  and tau levels, as well as decreases in regional glucose uptake, in all three diagnostic groups. We also observed *APOE*  $\epsilon$ 4-associated differences in the volumes of several brain regions in MCI and AD participants, as well as an *APOE*  $\epsilon$ 4-associated increase in total WMHS in CN participants. We did not observe any significant *APOE*  $\epsilon$ 4-associated differences in regional CBF levels when performing this diagnostic group-level analysis.

Perhaps not surprisingly, the most extensive differences between *APOE*  $\epsilon$ 4 carriers versus non-carriers that we observed were in regional  $A\beta$  levels. *APOE*  $\epsilon$ 4 carriers diagnosed as CN, MCI, and AD all displayed significantly increased  $A\beta$  accumulation in a vast array of brain regions (Figure 1B), the complete list of which are provided in Tables S2–S4 in supporting information. These include regions within the temporal, frontal, and parietal cortices, as well as the anterior and posterior cingulate cortex, the precuneus, the nucleus accumbens, and the insula. Medial temporal lobe (MTL) regions such as the parahippocampal cortex, the entorhinal cortex, and the amygdala also displayed significantly increased  $A\beta$  levels in *APOE*  $\epsilon$ 4 carriers versus non-carriers in each diagnostic group, although the effect sizes were relatively smaller in these regions.

The *APOE*  $\epsilon$ 4-associated differences in tau pathology that we observed in this diagnostic group-level analysis were not as robust as those observed for  $A\beta$ ; however, the regions that did display signifi-

**TABLE 1** Participant information for APOE4 analyses.

	CN, APOE4-	CN, APOE4+	MCI, APOE4-	MCI, APOE4+	AD, APOE4-	AD, APOE4+	p-value
<b>Aβ-PET</b>							
Participants (% of total)	349 (24.3)	156 (10.9)	329 (22.9)	269 (18.7)	126 (8.8)	207 (14.4)	
Visits (% of total)	877 (30.7)	383 (13.4)	677 (23.7)	477 (16.7)	165 (5.8)	279 (9.8)	
Visits per participant, mean (SD)	2.51 (1.46)	2.46 (1.39)	2.06 (1.23)	1.77 (1.1)	1.31 (0.7)	1.35 (0.56)	p<0.001
Sex, # of male (%)	163 (46.7)	55 (35.3)	178 (54.1)	158 (58.7)	77 (61.1)	116 (56)	p<0.001
Age at visit, mean (SD)	75.66 (7.01)	73.54 (6.88)	76.06 (8.03)	73.63 (7.19)	78.6 (8.74)	75.1 (7.59)	p<0.001
Age, # of 75+ yr olds (%)	220 (54)	82 (43)	207 (57)	129 (44)	92 (71)	114 (54)	p<0.001
Race/Ethnicity, # of non-Hispanic White (%)	286 (81.9)	121 (77.6)	294 (89.4)	246 (91.4)	111 (88.1)	189 (91.3)	p<0.001
Years of education, mean (SD)	16.72 (2.54)	16.38 (2.49)	16.06 (2.63)	16.05 (2.83)	16.17 (2.57)	15.77 (2.62)	0.001
<b>Tau-PET</b>							
Participants (% of total)	286 (34.7)	150 (18.2)	165 (20)	105 (12.7)	43 (5.2)	75 (9.1)	
Visits (% of total)	461 (34.7)	268 (20.2)	234 (17.6)	174 (13.1)	75 (5.6)	117 (8.8)	
Visits per participant, mean (SD)	1.61 (0.9)	1.79 (0.92)	1.42 (0.72)	1.66 (0.92)	1.74 (0.82)	1.56 (0.72)	0.004
Sex, # of male (%)	118 (41.3)	55 (36.7)	90 (54.5)	61 (58.1)	25 (58.1)	44 (58.7)	p<0.001
Age at visit, mean (SD)	74.11 (7.8)	71.75 (6.86)	75.6 (8.07)	73.8 (7.57)	78.2 (9.43)	75.66 (8.24)	p<0.001
Age, # of 75+ yr olds (%)	135 (44)	54 (33)	92 (55)	51 (47)	33 (73)	41 (53)	p<0.001
Race/Ethnicity, # of non-Hispanic White (%)	221 (77.3)	111 (74)	136 (82.4)	91 (86.7)	40 (93)	65 (86.7)	0.013
Years of education, mean (SD)	16.9 (2.31)	16.39 (2.25)	16.24 (2.56)	16.2 (2.71)	15.63 (2.7)	15.89 (2.41)	0.003
<b>FDG-PET</b>							
Participants (% of total)	325 (18.4)	123 (7)	453 (25.6)	390 (22.1)	163 (9.2)	313 (17.7)	
Visits (% of total)	725 (20.6)	259 (7.4)	906 (25.7)	780 (22.2)	285 (8.1)	566 (16.1)	
Visits per participant, mean (SD)	2.23 (1.71)	2.11 (1.64)	2 (1.63)	2 (1.59)	1.75 (1.15)	1.81 (1.19)	0.003
Sex, # of male (%)	161 (49.5)	52 (42.3)	260 (57.4)	229 (58.7)	104 (63.8)	179 (57.2)	0.002
Age at visit, mean (SD)	75.35 (6.31)	73.86 (6.14)	75.04 (7.94)	73.03 (6.9)	77.74 (8.61)	75.1 (7.3)	p<0.001
Age, # of 75+ yr olds (%)	181 (52)	60 (45)	246 (52)	174 (42)	117 (70)	167 (52)	p<0.001
Race/Ethnicity, # of non-Hispanic White (%)	283 (87.1)	104 (84.6)	399 (88.1)	354 (90.8)	147 (90.2)	280 (89.5)	0.485
Years of education, mean (SD)	16.46 (2.72)	16.3 (2.66)	16.02 (2.63)	15.91 (2.84)	15.8 (2.73)	15.55 (2.9)	0.003
<b>Structural MRI</b>							
Participants (% of total)	222 (21.7)	93 (9.1)	251 (24.5)	212 (20.7)	75 (7.3)	172 (16.8)	
Visits (% of total)	871 (21.9)	325 (8.2)	1191 (29.9)	958 (24.1)	176 (4.4)	458 (11.5)	
Visits per participant, mean (SD)	3.92 (1.87)	3.49 (1.73)	4.75 (2.53)	4.52 (2.17)	2.35 (1.42)	2.66 (1.46)	p<0.001
Sex, # of male (%)	104 (46.8)	35 (37.6)	137 (54.6)	126 (59.4)	47 (62.7)	95 (55.2)	0.003
Age at visit, mean (SD)	74.98 (6.4)	73.44 (6.59)	74.63 (8.17)	72.65 (7.09)	76.66 (8.82)	74.34 (7.19)	0.001
Age, # of 75+ yr olds (%)	125 (0.47)	46 (0.38)	149 (0.48)	97 (0.38)	53 (0.68)	88 (0.49)	0
Race/Ethnicity, # of non-Hispanic White (%)	188 (84.7)	78 (83.9)	231 (92)	194 (91.5)	66 (88)	158 (91.9)	0.043
Years of education, mean (SD)	16.57 (2.62)	16.41 (2.65)	16.05 (2.67)	15.99 (2.84)	16.04 (2.76)	15.76 (2.66)	0.052
<b>ASL MRI (CBF)</b>							
Participants (% of total)	101 (26.2)	47 (12.2)	94 (24.4)	63 (16.4)	24 (6.2)	56 (14.5)	
Visits (% of total)	203 (25.8)	87 (11)	225 (28.6)	148 (18.8)	30 (3.8)	95 (12.1)	
Visits per participant, mean (SD)	2.01 (1.26)	1.85 (1.02)	2.39 (1.6)	2.35 (1.32)	1.25 (0.74)	1.7 (0.93)	0.001
Sex, # of male (%)	44 (0.44)	22 (0.44)	56 (0.57)	36 (0.57)	13 (0.65)	33 (0.61)	0.14
Age at visit, mean (SD)	74.17 (6.9)	71.5 (7.42)	73.69 (8.63)	72.72 (6.65)	77.23 (6.58)	73.03 (6.5)	0.026
Age, # of 75+ yr olds (%)	50 (48)	17 (34)	46 (46)	23 (37)	21 (88)	22 (39)	p<0.001
Race/Ethnicity, # of non-Hispanic White (%)	86 (85.1)	41 (87.2)	86 (91.5)	57 (90.5)	22 (91.7)	50 (89.3)	0.77
Years of education, mean (SD)	16.8 (2.35)	16.11 (2.87)	16.44 (2.7)	16.35 (2.85)	16 (2.55)	16.36 (2.58)	0.77

(Continues)

**TABLE 1** (Continued)

	CN, APOE4-	CN, APOE4+	MCI, APOE4-	MCI, APOE4+	AD, APOE4-	AD, APOE4+	p-value
<b>FLAIR MRI (WMH)</b>							
Participants (% of total)	441 (25.8)	209 (12.2)	390 (22.8)	298 (17.4)	129 (7.5)	245 (14.3)	
Visits (% of total)	1474 (26.1)	649 (11.5)	1476 (26.2)	1130 (20)	287 (5.1)	621 (11)	
Visits per participant, mean (SD)	3.34 (2.39)	3.11 (2.18)	3.78 (2.55)	3.79 (2.34)	2.22 (1.34)	2.53 (1.37)	p<0.001
Sex, # of male (%)	194 (44)	79 (37.8)	211 (54.1)	171 (57.4)	79 (61.2)	136 (55.5)	p<0.001
Age at visit, mean (SD)	73.91 (7.24)	72.11 (6.6)	75.09 (8.21)	73.02 (7.15)	78.09 (8.89)	74.7 (7.33)	p<0.001
Age, # of 75+ yr olds (%)	227 (45)	85 (35)	228 (52)	140 (43)	97 (71)	129 (50)	p<0.001
Race/Ethnicity, # of non-Hispanic White (%)	356 (80.7)	164 (78.5)	337 (86.4)	268 (89.9)	115 (89.1)	220 (89.8)	p<0.001
Years of education, mean (SD)	16.75 (2.43)	16.49 (2.38)	16.01 (2.62)	16.11 (2.73)	15.85 (2.66)	15.71 (2.62)	p<0.001

Abbreviations: A $\beta$ , amyloid beta; AD, Alzheimer's disease; APOE, apolipoprotein E; ASL, arterial spin labeling; CBF, cerebral blood flow; CN, cognitively normal; FDG, fluorodeoxyglucose; FLAIR, fluid-attenuated inversion recovery; MCI, mild cognitive impairment; MRI, magnetic resonance imaging; PET, positron emission tomography; SD, standard deviation; WMH, white matter hyperintensity.

cant differences are very informative (Figure 1C and Tables S5–S7 in supporting information). In CN participants, only the amygdala and the entorhinal cortex showed significantly increased tau levels between APOE  $\epsilon$ 4 carriers versus non-carriers. In MCI participants, the amygdala and the entorhinal cortex were again the most significantly increased regions in APOE  $\epsilon$ 4 carriers, but many other regions, including the hippocampus and numerous temporal cortex regions, also showed significantly increased tau deposition, as well. While in AD participants, even more regions showed APOE  $\epsilon$ 4-associated increases in tau deposition, with temporal cortex regions such as the inferior temporal gyrus, the middle temporal gyrus, and the banks of the superior temporal sulcus (bankssts) being the most affected, and with regions in the frontal, parietal, and occipital cortices also showing significantly increased tau pathology in the APOE  $\epsilon$ 4 carriers. This suggests that APOE  $\epsilon$ 4-associated increases in tau pathology are most pronounced in the MTL and the temporal cortex, with increasing and more dispersed regional differences in tau pathology throughout AD progression, whereas the APOE  $\epsilon$ 4-associated increases in A $\beta$  pathology are more uniformly distributed throughout the brain, with the levels between APOE  $\epsilon$ 4 carriers versus non-carriers remaining relatively consistent from CN to MCI to AD.

Interestingly, we also observed significant APOE  $\epsilon$ 4-associated differences in CN, MCI, and AD participants for the glucose uptake measures recorded by FDG PET. For this FDG PET analysis, the investigators who performed this analysis chose to represent their data as one combined "MetaROI," which consists of the posterior cingulate cortex, the angular gyrus, and the inferior temporal gyrus. In our figures, this MetaROI is represented by the bilateral posterior cingulate cortex, the inferior parietal cortex (which includes the angular gyrus), and the inferior temporal cortex (which includes the inferior temporal gyrus). As shown in Figure 1D (and Tables S8–S10 in supporting information), glucose uptake is downregulated in the MetaROI of these brain regions in APOE  $\epsilon$ 4 carriers from all three diagnostic groups, with the effect size increasing from CN to MCI to AD.

Finally, while we did not observe any significant diagnostic group-level differences in the ASL MRI analysis, we did observe a significant APOE  $\epsilon$ 4-associated difference in MCI and AD participants for the structural MRI analysis and in CN participants for the FLAIR MRI analysis. As shown in Figure 1E (and Tables S11–S12 in supporting information), we observed decreased brain volume in the hippocampus, the entorhinal cortex, and the amygdala, as well as in the middle temporal gyrus, the fusiform gyrus, and the inferior parietal cortex of MCI APOE  $\epsilon$ 4 carriers, and we observed decreased brain volume in the hippocampus, the middle temporal gyrus, the fusiform gyrus, and the inferior parietal cortex of AD APOE  $\epsilon$ 4 carriers. Interestingly, we also observed increased volume of the inferior lateral ventricles of AD APOE  $\epsilon$ 4 carriers. For the WMH analyses, the investigators did not provide regional measurements, but instead only included one ROI label (TOTAL\_WMh) that represents any hyperintensities observed throughout the white matter; therefore, we have chosen to represent this in our figures using the entire cerebral white matter ROI. As shown in Figure 1F (and Table S13 in supporting information), the TOTAL\_WMh signal was significantly increased in CN APOE  $\epsilon$ 4 carriers.

### 3.2 | APOE $\epsilon$ 4-associated differences, stratified by sex

To investigate the sex-specific differences in each of these neuroimaging biomarkers, as a function of APOE  $\epsilon$ 4 carrier status, we performed the same analyses described above, but for the female or the male ADNI participants stratified separately. Importantly, female APOE  $\epsilon$ 4 carriers are at a greater risk of developing AD than male APOE  $\epsilon$ 4 carriers,<sup>24–26</sup> which we hypothesized would be reflected in the AD-related pathology present in the brains of female versus male ADNI participants. As displayed in Figure 2A, this sex-stratified analysis revealed some interesting results. In regard to A $\beta$  pathology, both the female and the male CN and MCI participants displayed significant APOE  $\epsilon$ 4-associated differences in similar brain regions as those that

## APOE4-associated Differences by Diagnostic Group

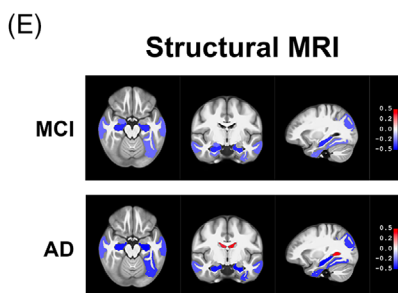
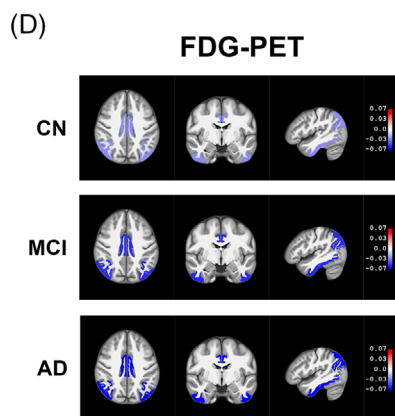
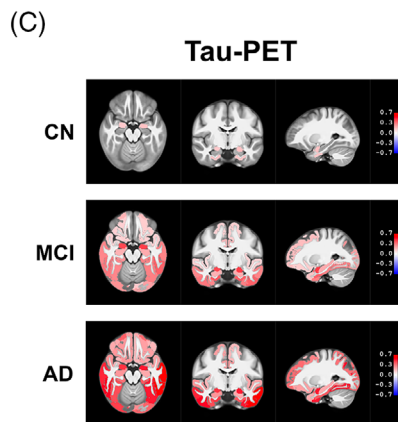
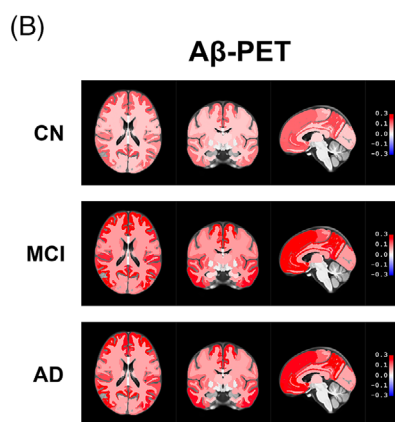
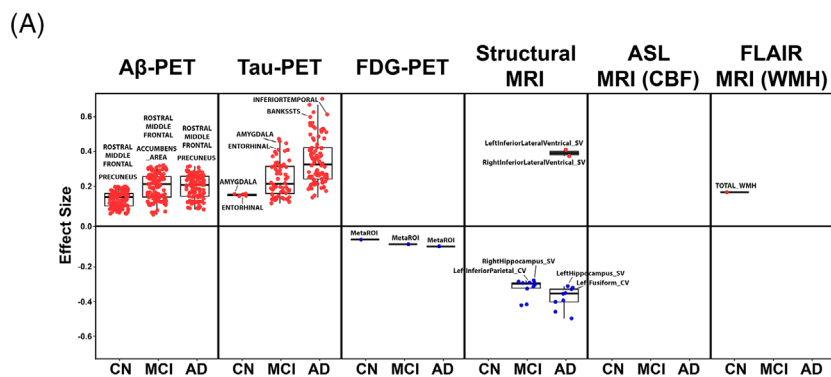


**FIGURE 1** APOE  $\epsilon 4$ -associated differences by diagnostic group. We performed linear mixed-effects analyses comparing regional neuroimaging biomarker levels between APOE  $\epsilon 4$  carriers versus non-carriers, classified into one of three diagnostic groups: CN, MCI, or AD participants. Regions with significantly different biomarker levels ( $p < 0.05$ ) between the APOE  $\epsilon 4$  carriers and non-carriers in each diagnostic group were graphed onto box plots with two of the top regions labeled (A). We also rendered the regions onto a human brain template (displayed axially, coronally, and sagittally) using different shades of red (upregulated in APOE  $\epsilon 4$  carriers) or blue (downregulated in APOE  $\epsilon 4$  carriers) that corresponds to the magnitude of their statistical difference (beta) between APOE  $\epsilon 4$  carrier groups (B)–(F). We show the rendered biomarker differences from each analysis that resulted in at least one statistically different region, which in this diagnostic group-level comparison included A $\beta$  PET results (B), tau PET results (C), FDG PET results (D), structural MRI results (E), and FLAIR MRI WMH results (F). A $\beta$ , amyloid beta; AD, Alzheimer's disease; APOE, apolipoprotein E; ASL, arterial spin labeling; CBF, cerebral blood flow; CN, cognitively normal; FDG, fluorodeoxyglucose; FLAIR, fluid-attenuated inversion recovery; MCI, mild cognitive impairment; MRI, magnetic resonance imaging; PET, positron emission tomography; WMH, white matter hyperintensity

we observed in the non-stratified analysis; however, we did observe a greater number of significant regions in the female CN APOE  $\epsilon 4$  carriers and larger effect sizes in the female MCI APOE  $\epsilon 4$  carriers (compared to female CN and MCI APOE  $\epsilon 4$  non-carriers) than we observed in the male CN and MCI APOE  $\epsilon 4$  carriers (compared to male CN and MCI

APOE  $\epsilon 4$  non-carriers; Figure 2B and Tables S14–S17 in supporting information).

For the tau PET measurements, we observed significant APOE  $\epsilon 4$ -associated tau pathology increases in the entorhinal cortex and the amygdala of the female CN participants, but not in the male CN partic-

## APOE4-associated Differences, Stratified by Sex

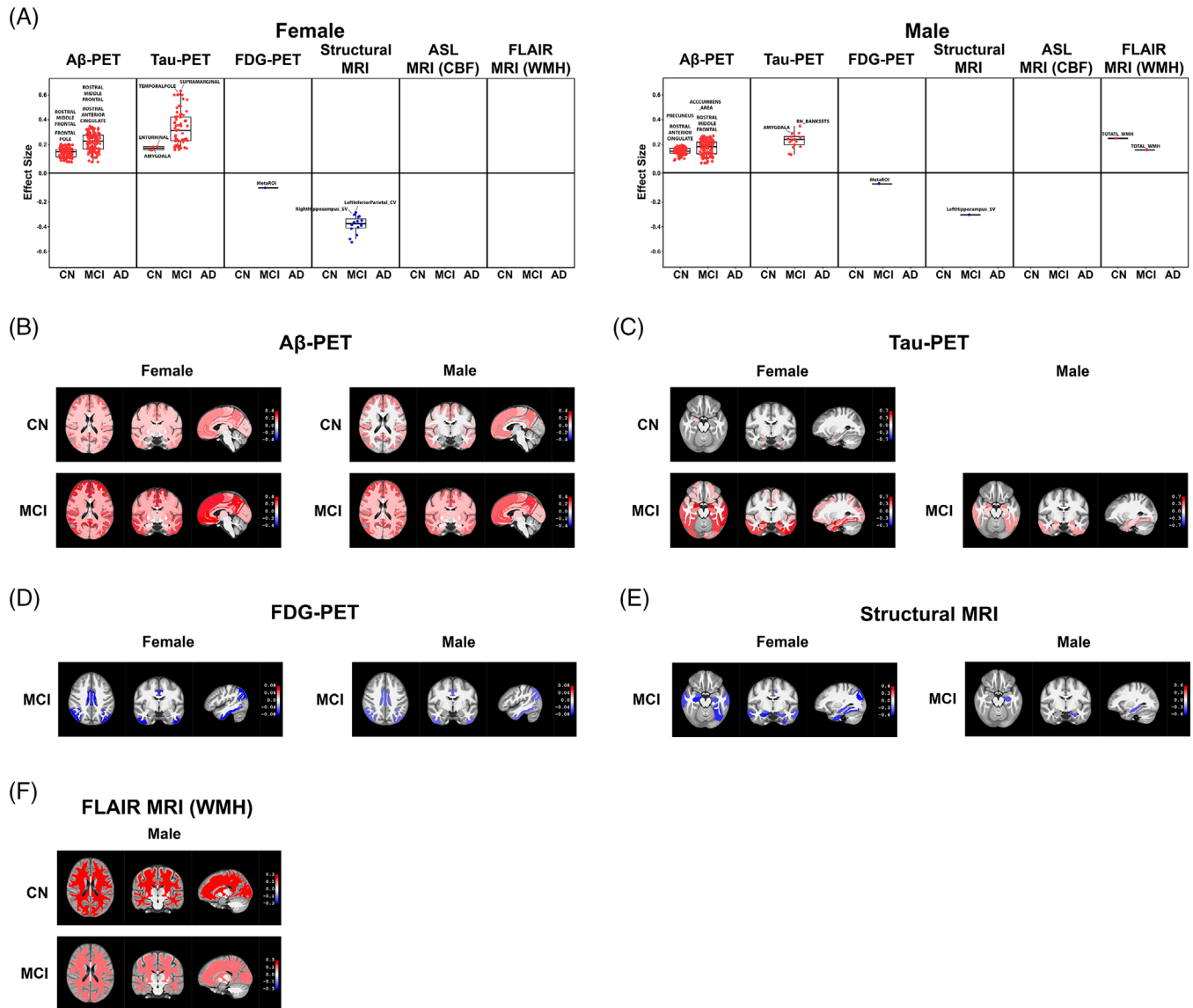


**FIGURE 2** APOE  $\epsilon 4$ -associated differences, stratified by sex. We performed linear mixed-effects analyses comparing regional neuroimaging biomarker levels between either female APOE  $\epsilon 4$  carriers versus female APOE  $\epsilon 4$  non-carriers or male APOE  $\epsilon 4$  carriers versus male APOE  $\epsilon 4$  non-carriers, again within each diagnostic group: CN, MCI, or AD participants. Regions with significantly different biomarker levels ( $p < 0.05$ ) between the APOE  $\epsilon 4$  carriers and non-carriers of each sex and within each diagnostic group were graphed onto box plots with two of the top regions labeled (A). We also rendered the regions onto a human brain template (displayed axially, coronally, and sagittally) using different shades of red (upregulated in APOE  $\epsilon 4$  carriers) or blue (downregulated in APOE  $\epsilon 4$  carriers) that corresponds to the magnitude of their statistical difference (beta) between APOE  $\epsilon 4$  carrier groups (B)–(F). Here we show the rendered biomarker differences from each analysis that resulted in at least one statistically different region, which in this sex stratification included A $\beta$  PET results (B), tau PET results (C), FDG PET results (D), structural MRI results (E), and FLAIR MRI WMH results (F). A $\beta$ , amyloid beta; AD, Alzheimer's disease; APOE, apolipoprotein E; ASL, arterial spin labeling; CBF, cerebral blood flow; CN, cognitively normal; FDG, fluorodeoxyglucose; FLAIR, fluid attenuated inversion recovery; MCI, mild cognitive impairment; MRI, magnetic resonance imaging; PET, positron emission tomography; WMH, white matter hyperintensity

ipants (Figure 2C and Tables S18–S20 in supporting information) while in MCI participants, we observed significant APOE  $\epsilon 4$ -associated tau pathology increases in both female and male APOE  $\epsilon 4$  carriers, although more regions and larger effect sizes were observed in the female MCI participants.

We also observed significant sex-specific APOE  $\epsilon 4$  differences in the FDG PET, structural MRI, and FLAIR MRI measurements. In both female and male MCI participants, the MetaROI FDG PET signal was

significantly downregulated in the APOE  $\epsilon 4$  carriers, with a larger effect size observed in the female MCI APOE  $\epsilon 4$  carriers (Figure 2D and Tables S21–S22 in supporting information). For the structural MRI analysis, the female MCI participants displayed significant APOE  $\epsilon 4$ -associated volume decreases in several regions, including the hippocampus, the amygdala, the posterior cingulate cortex, and the precuneus, and the male MCI APOE  $\epsilon 4$  participants displayed decreased volume in the left hippocampus (Figure 2E and Tables S23–S24 in supporting informa-

tion). Interestingly, the *APOE*  $\epsilon 4$ -associated differences in the FLAIR MRI analysis were the one result that was specific to the male *APOE*  $\epsilon 4$  participants, with both male CN *APOE*  $\epsilon 4$  participants and male MCI *APOE*  $\epsilon 4$  participants showing a significantly increased TOTAL\_WMh signal compared to their *APOE*  $\epsilon 4$  non-carrier counterparts (Figure 2F and Tables S25–S26 in supporting information).

Overall, these sex-stratified analyses suggest that female *APOE*  $\epsilon 4$  carriers possess relatively higher levels of AD-related pathology (compared to non-carriers) than do male *APOE*  $\epsilon 4$  carriers, especially during MCI. A notable exception, however, appears to be WMHs, which were only observed in male CN and MCI *APOE*  $\epsilon 4$  carriers (compared to male CN and MCI *APOE*  $\epsilon 4$  non-carriers).

### 3.3 | *APOE* $\epsilon 4$ -associated differences, stratified by age

We also performed this analysis using age, instead of sex, for the stratification (Figure 3). We chose an age of 75 years as a relative midpoint between the younger and the older ADNI participants (the majority of whom are between 60 and 90 years old). *APOE*  $\epsilon 4$  is known to have some important age-related effects: *APOE*  $\epsilon 4$  carriers generally display an earlier age of AD onset than *APOE*  $\epsilon 4$  non-carriers, and the overall risk associated with *APOE*  $\epsilon 4$  is higher in younger *APOE*  $\epsilon 4$  carriers, with the peak odds ratio in White *APOE*  $\epsilon 4$  carriers reported to occur at  $\approx 65$  years old in *APOE*  $\epsilon 3/\epsilon 4$  carriers and at  $\approx 60$  years old in *APOE*  $\epsilon 4/\epsilon 4$  carriers.<sup>24</sup> For this analysis, the biomarker measurements for each participant were taken separately from the visits performed while the participants were < 75 years old and again from the visits performed while the participants were  $\geq 75$  years old, and each of these visit groupings were used for the two separate age-stratified analyses.

Overall, there were a mix of biomarkers and regions that displayed significant *APOE*  $\epsilon 4$ -associated differences in each age group (Figure 3A). For the  $A\beta$  PET measurements, we observed similar *APOE*  $\epsilon 4$ -associated differences in both the under-75 and the 75-and-over ADNI visits, with both age groups showing similar brain-wide increases in  $A\beta$  between *APOE*  $\epsilon 4$  carriers versus non-carriers for both CN and MCI participants (Figure 3B and Tables S27–S30 in supporting information). This was not the case for the tau PET measurements, however. While we only observed significant *APOE*  $\epsilon 4$ -associated differences in tau pathology in the MCI participants during this age stratification analysis, the under-75 MCI *APOE*  $\epsilon 4$  carriers versus non-carriers possessed more regions of significantly increased tau pathology, as well as larger effect sizes, than the 75-and-over MCI *APOE*  $\epsilon 4$  carriers versus non-carriers (Figure 3C and Tables S31–S32 in supporting information).

We also observed age-specific differences in CN and MCI participants for the FDG PET measurements, with 75-and-over CN *APOE*  $\epsilon 4$  carriers and both under-75 and 75-and-over MCI *APOE*  $\epsilon 4$  carriers displaying decreased glucose uptake in the MetaROI regions compared to their *APOE*  $\epsilon 4$  non-carrier counterparts (Figure 3D and Tables S33–S35 in supporting information). In addition, for the structural MRI analysis, we observed decreased volume of the hippocampus and increased

volume of the inferior lateral ventricles and the left lateral ventricle in under-75 MCI *APOE*  $\epsilon 4$  carriers, as well as decreased volume of the hippocampus, the entorhinal cortex, and several other brain regions in 75-and-over MCI *APOE*  $\epsilon 4$  carriers (Figure 3E and Tables S36–S37 in supporting information). We also observed an intriguing decrease in CBF levels in a number of brain regions in the under-75 CN *APOE*  $\epsilon 4$  carriers, including in the nucleus accumbens, the left hippocampus, the right parahippocampal cortex, and the thalamus (Figure 3F and Table S38 in supporting information). And last, we observed a significantly increased TOTAL\_WMh signal, as measured by FLAIR MRI, in the 75-and-over CN *APOE*  $\epsilon 4$  carriers (Figure 3G and Table S39 in supporting information).

### 3.4 | Conversion status, stratified by *APOE* $\epsilon 4$ possession

As a final analysis, we took advantage of the longitudinal nature of ADNI and investigated whether there are differences in these neuroimaging biomarkers between CN participants who converted to MCI or AD over the course of their ADNI participation versus those who did not convert to MCI or AD during their ADNI participation. In this analysis, converter status (CN→MCI/AD vs. CN→CN) was used as the independent variable, and the regional levels of pathology were again used as the dependent variables, with each analysis performed separately in *APOE*  $\epsilon 4$  carriers or in *APOE*  $\epsilon 4$  non-carriers. Once again, each analysis was controlled for sex and age of the participants. Importantly, these results should be viewed as preliminary, as the numbers of CN participants who later converted to MCI/AD and also possessed data from any of these six neuroimaging datasets, especially in the tau PET and the ASL MRI datasets, were relatively small (please see Table 2 for the numbers and demographic information of the converters and non-converters for each analysis).

As shown in Figure 4A, we observed significant regional differences between the converters and the non-converters, in an *APOE*  $\epsilon 4$ -dependent fashion, in five separate biomarker measurements:  $A\beta$  PET, tau PET, FDG PET, structural MRI, and FLAIR MRI. For  $A\beta$  PET, we observed significantly increased  $A\beta$  levels in CN *APOE*  $\epsilon 4$  carriers who converted to MCI/AD (compared to CN *APOE*  $\epsilon 4$  carriers who did not convert) in several brain regions, including the anterior cingulate cortex, the nucleus accumbens, and the superior frontal cortex (Figure 4B and Table S40 in supporting information). For tau PET, we observed significantly increased tau pathology in the amygdala and in temporal cortex regions such as the middle temporal gyrus, the fusiform gyrus, and bankssts in CN *APOE*  $\epsilon 4$  non-carriers who converted to MCI/AD (compared to CN *APOE*  $\epsilon 4$  non-carriers who did not convert), while CN *APOE*  $\epsilon 4$  carrier converters showed increased tau pathology in broader temporal, frontal, and parietal cortex regions, as well as in the anterior cingulate cortex (Figure 4C and Tables S41–S42 in supporting information).

For FDG PET, only the *APOE*  $\epsilon 4$  non-carrier converters displayed significantly different MetaROI signals than non-converters, with decreased glucose uptake observed in the brains of these converters

## APOE4-associated Differences, Stratified by Age

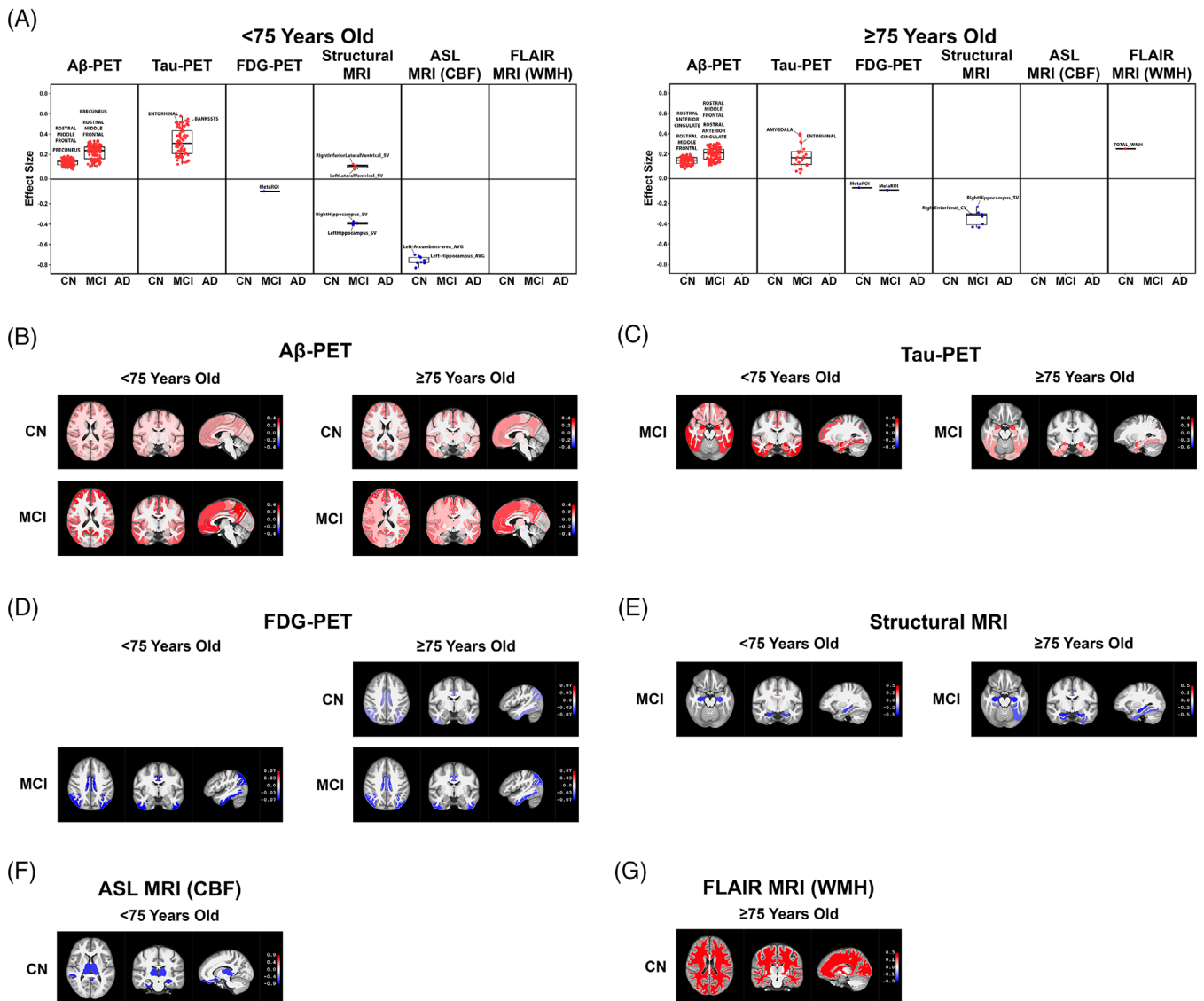


**FIGURE 3** APOE  $\epsilon 4$ -associated differences, stratified by age. We performed linear mixed-effects analyses comparing regional neuroimaging biomarker levels between either under-75 APOE  $\epsilon 4$  carriers versus under-75 APOE  $\epsilon 4$  non-carriers or 75-and-over APOE  $\epsilon 4$  carriers versus 75-and-over APOE  $\epsilon 4$  non-carriers, again within each diagnostic group: CN, MCI, or AD participants. Regions with significantly different biomarker levels ( $p < 0.05$ ) between the APOE  $\epsilon 4$  carriers and non-carriers from each age group and within each diagnostic group were graphed onto box plots with two of the top regions labeled (A). We also rendered the regions onto a human brain template (displayed axially, coronally, and sagittally) using different shades of red (upregulated in APOE  $\epsilon 4$  carriers) or blue (downregulated in APOE  $\epsilon 4$  carriers) that corresponds to the magnitude of their statistical difference (beta) between APOE  $\epsilon 4$  carrier groups (B)–(G). Here we show the rendered biomarker differences from each analysis that resulted in at least one statistically different region, which in this age stratification included A $\beta$  PET results (B), tau PET results (C), FDG PET results (D), structural MRI results (E), ASL MRI CBF results (F), and FLAIR MRI WMH results (G). A $\beta$ , amyloid beta; AD, Alzheimer's disease; APOE, apolipoprotein E; ASL, arterial spin labeling; CBF, cerebral blood flow; CN, cognitively normal; FDG, fluorodeoxyglucose; FLAIR, fluid attenuated inversion recovery; MCI, mild cognitive impairment; MRI, magnetic resonance imaging; PET, positron emission tomography; WMH, white matter hyperintensity

(Figure 4D and Table S43 in supporting information). For structural MRI, APOE  $\epsilon 4$  non-carrier converters displayed significantly increased volumes of their inferior lateral ventricles compared to non-converters (Figure 4E and Table S44 in supporting information). And for FLAIR MRI, we observed significant increases in TOTAL\_WMh signal in both the APOE  $\epsilon 4$  non-carrier and the APOE  $\epsilon 4$  carrier CN participants

who converted to MCI/AD, compared to those who did not convert (Figure 4F and Tables S45–S46 in supporting information).

These results, though underpowered, suggest that there may be regional differences in several neuroimaging biomarkers observed in elderly, cognitively unimpaired individuals that can signal an increased risk of developing MCI or AD, and that these biomarker signals may be different depending on the individual's APOE  $\epsilon 4$  carrier sta-

**TABLE 2** Participant information for converter status analyses.

	NC, APOE4-	NC, APOE4+	C, APOE4-	C, APOE4+	p-value
<b>Aβ-PET</b>					
Participants (% of total)	298 (61.3)	122 (25.1)	40 (8.2)	26 (5.3)	
Visits (% of total)	798 (64.6)	322 (26.1)	63 (5.1)	52 (4.2)	
Visits per participant, mean (SD)	2.68 (1.49)	2.64 (1.42)	1.57 (0.75)	2 (1.1)	p<0.001
Sex, # of male (%)	138 (46.3)	38 (31.1)	21 (52.5)	16 (61.5)	0.008
Age at visit, mean (SD)	75.41 (6.99)	73.12 (6.64)	78.24 (5.71)	77.88 (5.38)	p<0.001
Age, # of 75+ yr olds (%)	186 (52)	61 (40)	29 (71)	20 (67)	0.001
Race/Ethnicity, # of non-Hispanic White (%)	248 (83.2)	96 (78.7)	33 (82.5)	24 (92.3)	0.382
Years of education, mean (SD)	16.82 (2.48)	16.34 (2.47)	15.78 (2.9)	16.5 (2.73)	0.073
<b>Tau-PET</b>					
Participants (% of total)	260 (63.7)	133 (32.6)	10 (2.5)	5 (1.2)	
Visits (% of total)	432 (62)	249 (35.7)	10 (1.4)	6 (0.9)	
Visits per participant, mean (SD)	1.66 (0.92)	1.87 (0.94)	1 (0)	1.2 (0.45)	0.003
Sex, # of male (%)	111 (42.7)	48 (36.1)	2 (20)	3 (60)	0.375
Age at visit, mean (SD)	74.34 (7.63)	72.14 (6.61)	74.89 (8.4)	76.37 (5.66)	0.053
Age, # of 75+ yr olds (%)	128 (46)	51 (35)	2 (20)	2 (40)	0.077
Race/Ethnicity, # of non-Hispanic White (%)	210 (80.8)	106 (79.7)	9 (90)	5 (100)	0.077
Years of education, mean (SD)	16.97 (2.28)	16.44 (2.34)	15.4 (2.88)	14.8 (1.3)	0.019
<b>FDG-PET</b>					
Participants (% of total)	261 (59.5)	87 (19.8)	57 (13)	34 (7.7)	
Visits (% of total)	574 (59.6)	180 (18.7)	135 (14)	74 (7.7)	
Visits per participant, mean (SD)	2.2 (1.71)	2.07 (1.67)	2.37 (1.71)	2.18 (1.6)	0.646
Sex, # of male (%)	125 (47.9)	33 (37.9)	33 (57.9)	19 (55.9)	0.214
Age at visit, mean (SD)	74.85 (6.32)	72.64 (6.04)	77.88 (5.46)	76.99 (5.07)	p<0.001
Age, # of 75+ yr olds (%)	137 (49)	34 (36)	42 (68)	25 (68)	p<0.001
Race/Ethnicity, # of non-Hispanic White (%)	226 (86.6)	72 (82.8)	50 (87.7)	31 (91.2)	0.646
Years of education, mean (SD)	16.57 (2.7)	16.21 (2.7)	15.88 (2.84)	16.38 (2.58)	0.456
<b>Structural MRI</b>					
Participants (% of total)	190 (61.5)	72 (23.3)	28 (9.1)	19 (6.1)	
Visits (% of total)	772 (65.8)	252 (21.5)	86 (7.3)	64 (5.5)	
Visits per participant, mean (SD)	4.06 (1.85)	3.5 (1.73)	3.07 (1.63)	3.37 (1.77)	0.028
Sex, # of male (%)	89 (46.8)	22 (30.6)	13 (46.4)	13 (68.4)	0.028
Age at visit, mean (SD)	74.59 (6.3)	72.96 (6.77)	77.34 (6.38)	75.44 (5.52)	0.028
Age, # of 75+ yr olds (%)	95 (47)	30 (37)	18 (62)	12 (52)	0.112
Race/Ethnicity, # of non-Hispanic White (%)	162 (85.3)	60 (83.3)	22 (78.6)	17 (89.5)	0.738
Years of education, mean (SD)	16.74 (2.56)	16.24 (2.58)	15.21 (2.71)	17.05 (2.82)	0.028
<b>ASL MRI (CBF)</b>					
Participants (% of total)	91 (62.3)	44 (30.1)	8 (5.5)	3 (2.1)	
Visits (% of total)	182 (63.2)	79 (27.4)	19 (6.6)	8 (2.8)	
Visits per participant, mean (SD)	2 (1.23)	1.8 (0.98)	2.38 (1.69)	2.67 (1.53)	0.901
Sex, # of male (%)	40 (44)	18 (40.9)	2 (25)	2 (66.7)	0.901
Age at visit, mean (SD)	74.01 (6.57)	71.14 (7.41)	76.2 (6.46)	76.8 (6.32)	0.146
Age, # of 75+ yr olds (%)	44 (46)	15 (33)	5 (62)	2 (50)	0.29
Race/Ethnicity, # of non-Hispanic White (%)	79 (86.8)	38 (86.4)	6 (75)	3 (100)	0.901
Years of education, mean (SD)	17.07 (2.19)	16.2 (2.87)	13.5 (1.41)	14.67 (3.06)	0.004

(Continues)

**TABLE 2** (Continued)

	NC, APOE4-	NC, APOE4+	C, APOE4-	C, APOE4+	p-value
<b>FLAIR MRI (WMH)</b>					
Participants (% of total)	388 (62)	179 (28.6)	39 (6.2)	20 (3.2)	
Visits (% of total)	1349 (64.8)	553 (26.6)	102 (4.9)	78 (3.7)	
Visits per participant, mean (SD)	3.48 (2.43)	3.09 (2.19)	2.62 (1.76)	3.9 (2.22)	0.102
Sex, # of male (%)	172 (44.3)	62 (34.6)	17 (43.6)	14 (70)	0.019
Age at visit, mean (SD)	73.86 (7.09)	71.9 (6.48)	76.16 (6.83)	75.47 (5.44)	0.001
Age, # of 75+ yr oldss (%)	201 (45)	69 (33)	21 (51)	13 (52)	0.02
Race/Ethnicity, # of non-Hispanic White (%)	319 (82.2)	143 (79.9)	32 (82.1)	18 (90)	0.709
Years of education, mean (SD)	16.86 (2.4)	16.46 (2.34)	15.56 (2.58)	17 (2.75)	0.01

Abbreviations: A $\beta$ , amyloid beta; AD, Alzheimer's disease; APOE, apolipoprotein E; ASL, arterial spin labeling; C, converter; CBF, cerebral blood flow; CN, cognitively normal; FDG, fluorodeoxyglucose; FLAIR, fluid-attenuated inversion recovery; MCI, mild cognitive impairment; MRI, magnetic resonance imaging; NC, non-converter; PET, positron emission tomography; SD, standard deviation; WMH, white matter hyperintensity.

tus. Specifically, in APOE  $\epsilon$ 4 carriers, increased A $\beta$  pathology in the anterior cingulate cortex, the nucleus accumbens, and the superior frontal cortex, increased tau pathology in the anterior cingulate cortex and broadly in the temporal, frontal, and parietal cortices, and increased WMHs in the brain may signal an increased risk of developing MCI or AD, while in APOE  $\epsilon$ 4 non-carriers, increased tau pathology in several temporal cortex regions, decreased glucose uptake in DMN regions, increased volume of the lateral inferior ventricles, and increased WMHs in the brain may signal increased risk of developing MCI or AD. However, additional studies using larger cohorts of CN to MCI/AD converters are required to validate and expand upon these findings.

### 3.5 | Using machine learning to predict CN to MCI/AD conversion

One exciting possibility from this type of analysis is the idea that either individual or combined neuroimaging biomarkers could potentially be used to predict the future MCI/AD conversion of a cognitively unimpaired individual, which could inform the use of a potential intervention strategy. To test this possibility with the ADNI datasets used in our study, we conducted a machine learning experiment that focused specifically on the neuroimaging biomarker regions identified in the conversion analysis above. Specifically, we asked whether weighted combinations of these regional neuroimaging biomarker measurements could predict conversion from CN to MCI/AD, either independent of APOE genotype or in an APOE genotype-dependent fashion. It should be noted, however, that for this analysis, we were even more limited by the number of available CN to MCI/AD converters available in these ADNI datasets. In order to test different combinations of regional biomarker signals, we could only use data from CN converters who had undergone scans from each of the different neuroimaging modalities prior to conversion to MCI/AD, and ultimately very few of the converters met this requirement. For this reason, we view this analysis as a proof-of-concept experiment, with

further study required using neuroimaging data from larger cohorts of converters.

Because of these limited numbers, we first considered the level of overlap between recorded visits of participants who converted from CN to MCI/AD across the six modalities. As shown in Figure 5A, we observed that most of the overlap existed in data from four of the six modalities (A $\beta$  PET, FDG PET, structural MRI, and FLAIR MRI), with very little overlap existing in participants who had undergone tau PET and ASL MRI scans. Therefore, we limited our machine learning experiment to these four modalities.

For both the converters and the non-converters, we selected and prioritized the earliest visit for any CN participant that contained data from all four modalities from the same visit. The final intersection size and the total number of records for this analysis was 213 participants, 35 of whom (16.4%) showed future records with at least one MCI or AD diagnosis. This included five converters who had separate modalities performed during different CN visits, which we included in our analysis to maximize the number of available converters. In total, we used the combined neuroimaging data from one visit per participant from 13 APOE  $\epsilon$ 4 carrier converters, 22 APOE  $\epsilon$ 4 non-carrier converters, 48 APOE  $\epsilon$ 4 carrier non-converters, and 130 APOE  $\epsilon$ 4 non-carrier non-converters (Figure 5B). Importantly, we split the data from each of these groups into our training set and our test set, using an  $\approx$  60/40 split for the training set/test set from each group.

As described further in the Methods section, we used the h2o package to conduct a rigorous supervised learning trial. To limit the number of features used in this analysis, which might cause overfitting, we chose to include seven non-redundant, significantly different ROIs identified in the previous converter analysis from the A $\beta$  PET, FDG PET, structural MRI, and FLAIR MRI analyses. These ROIs were CAUDALANTERIORCINGULATE, LH\_ROSTRALANTERIORCINGULATE, LEFT\_ACCUMBENS\_AREA, and SUPERIORFRONTAL from the A $\beta$  PET analysis, MetaROI from the FDG PET analysis, RightInferiorLateralVentricle\_SV from the structural MRI analysis, and TOTAL\_WMh from the FLAIR MRI analysis. We then used the h2o.automl function to randomly fit 40 different machine learning models onto the data.

## Converter Status, Stratified by APOE4 Possession

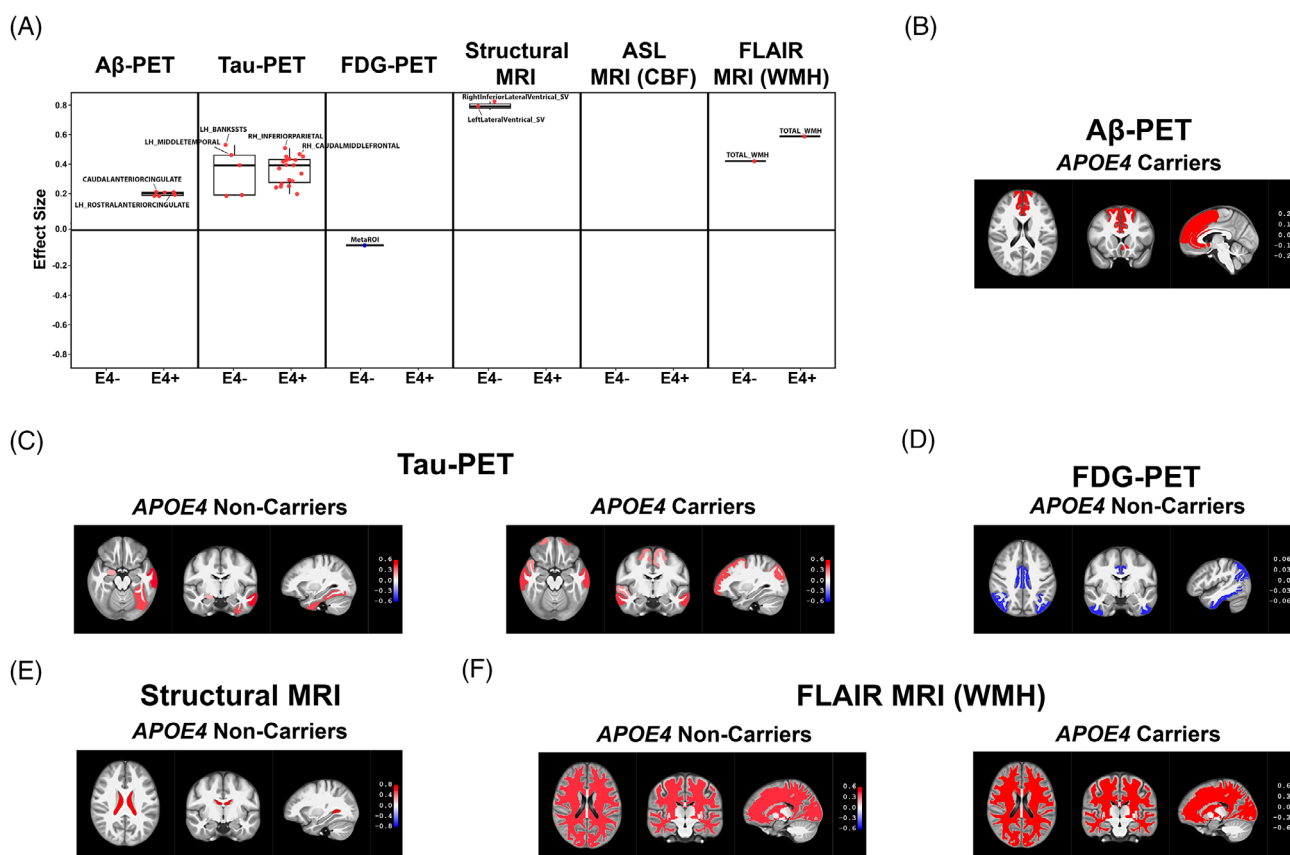


**FIGURE 4** Converter status, stratified by APOE  $\epsilon 4$  possession. We performed linear mixed-effects analyses comparing regional neuroimaging biomarker levels between APOE  $\epsilon 4$  non-carrier or APOE  $\epsilon 4$  carrier CN participants who converted to MCI or AD over the course of their ADNI participation versus APOE  $\epsilon 4$  non-carrier or APOE  $\epsilon 4$  carrier CN participants who did not convert to MCI or AD during their ADNI participation, again within each diagnostic group: CN, MCI, or AD participants. Regions with significantly different biomarker levels ( $p < 0.05$ ) between the converters and non-converters from each APOE  $\epsilon 4$  carrier group and within each diagnostic group were graphed onto box plots with two of the top regions labeled (A). We also rendered the regions onto a human brain template (displayed axially, coronally, and sagittally) using different shades of red (upregulated in APOE  $\epsilon 4$  carriers) or blue (downregulated in APOE  $\epsilon 4$  carriers) that corresponds to the magnitude of their statistical difference (beta) between converter status groups (B)–(F). Here we show the rendered biomarker differences from each analysis that resulted in at least one statistically different region, which in this converter status comparison included Aβ PET results (B), tau PET results (C), FDG PET results (D), structural MRI results (E), and FLAIR MRI WMH results (F). Aβ, amyloid beta; AD, Alzheimer's disease; APOE, apolipoprotein E; ASL, arterial spin labeling; CBF, cerebral blood flow; CN, cognitively normal; FDG, fluorodeoxyglucose; FLAIR, fluid attenuated inversion recovery; MCI, mild cognitive impairment; MRI, magnetic resonance imaging; PET, positron emission tomography; WMH, white matter hyperintensity.

As shown in Figure 5C, four of these models performed the best, and of these four, two of the models used an Extreme Gradient Boosted (XGBoost) algorithm, which creates an ensemble of several weak learners, usually decision trees, to create a more accurate prediction tool.<sup>27</sup> We therefore opted to train the XGBoosted algorithm using the seven ROIs listed above. We fitted 50 models based on random combinations of a grid of hyperparameter values. For each model, we used 3-fold cross-validation.

Interestingly, each of these 50 models generated by the trained XGBoosted algorithm possessed highly weighted contributions from two top ROIs (MetaROI from the FDG PET analysis and RightInferiorLateralVentricle\_SV from the structural MRI analysis; Figure 5D), with both ROIs contributing  $\approx 20\%$  each to most of the models' overall conversion prediction performance. TOTAL\_WM from the FLAIR

MRI analysis also showed a large contribution to many of the models, with the Aβ PET measures contributing the least to most of the models. Judging from the direction of the differences in these ROIs displayed in Figure 4, this result suggests that the decreased glucose uptake and the increased ventricle size observed in the converters, as well as the increased presence of WMHs, were the greatest determinants of the CN participants' future conversion to MCI/AD, as generated by these XGBoosted models.

We next compared the performance metrics for all 50 models across each of the training and test sets (Figure 5E and Table S47 in supporting information). Across three separate performance metrics (AUC, AUC-PR, and log-loss), we observed similar results for each of the 50 XGBoosted models. Overall, the combined test set and the APOE  $\epsilon 4$  non-carrier test set performed similarly, with the combined

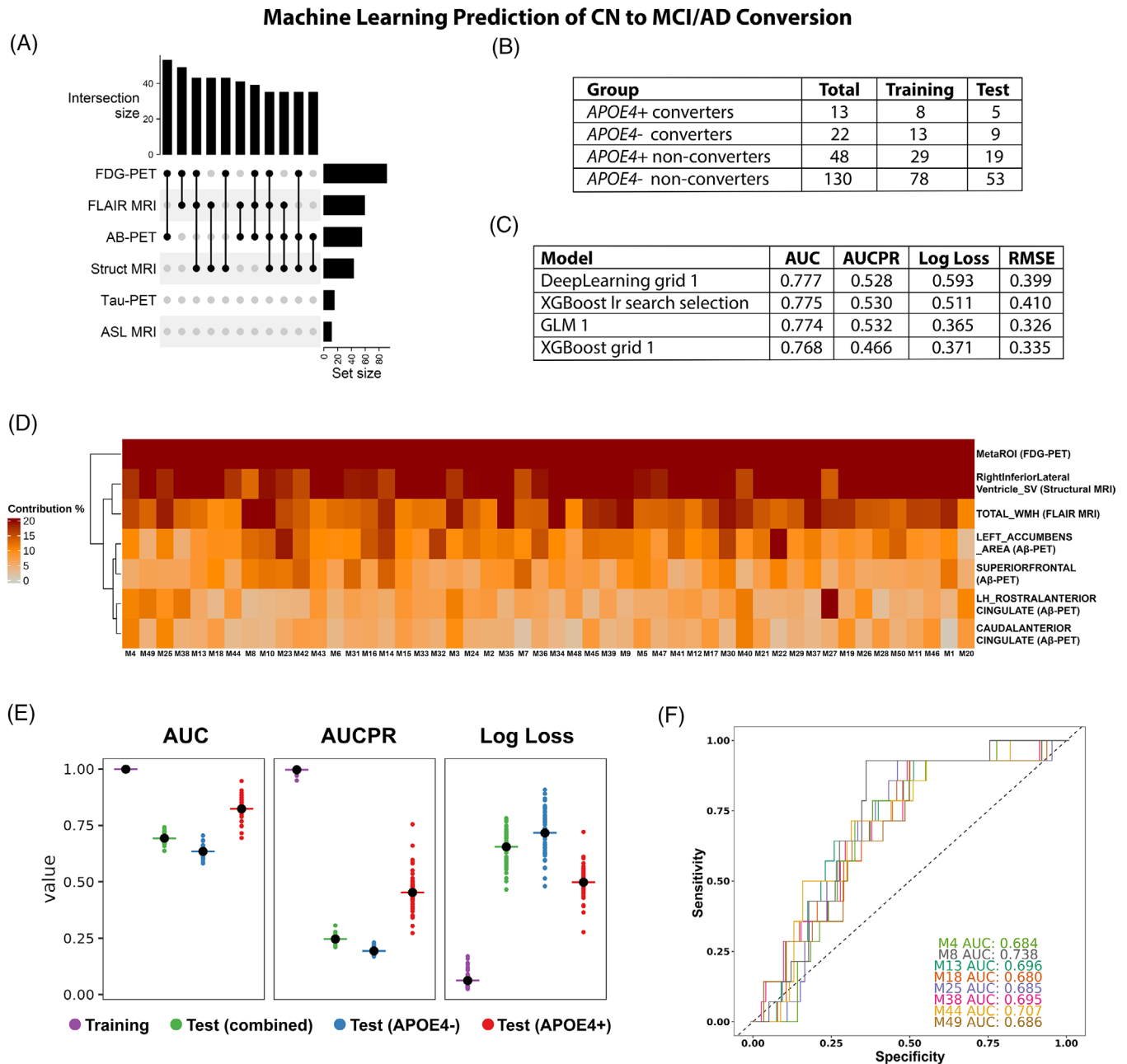


**FIGURE 5** Machine learning prediction of CN to MCI/AD conversion. We performed a machine learning experiment to investigate whether the biomarker regions identified in our conversion analysis could be used to predict future MCI/AD conversion in cognitively unimpaired individuals. A, An upset plot used to determine the amount of participant data overlap for each neuroimaging modality. B, The participant numbers, characteristics, and training versus test set assignments for all participants with overlapping data from the  $A\beta$  PET, FDG PET, structural MRI, and FLAIR MRI analyses. C, Performance metrics, including AUC, AUCPR, log-loss, and RMSE, of the top 4 (out of 40) machine learning models tested from the h2o package. D, The contribution matrix of all 50 models generated by the trained XGBoosted algorithm. E, Performance metrics for all 50 models across the training set and each of the test sets (combined, *APOE*  $\epsilon 4^-$ , and *APOE*  $\epsilon 4^+$ ). F, AUC ROC curves from the combined test set using the eight models with the lowest log-loss scores from the training set.  $A\beta$ , amyloid beta; AD, Alzheimer's disease; ASL, arterial spin labeling; AUC, area under the curve; AUCPR, area under the precision-recall curve; CBF, cerebral blood flow; CN, cognitively normal; FDG, fluorodeoxyglucose; FLAIR, fluid attenuated inversion recovery; MCI, mild cognitive impairment; MRI, magnetic resonance imaging; PET, positron emission tomography; RMSE, root mean squared error; ROC, receiver operator characteristic; WMH, white matter hyperintensity

test set performing slightly better (with a mean AUC of 0.69) than the APOE  $\epsilon$ 4 non-carrier test set (mean AUC 0.63). Interestingly, looking at the metrics from the APOE  $\epsilon$ 4 carrier test set, we observed increased variance among the performance of the 50 XGBoosted models, as well as a robust increase in the performance of the models overall (mean AUC 0.82). However, this result should be interpreted with caution, given the low number of APOE  $\epsilon$ 4 carrier converters used for this experiment. Last, as a visual demonstration of the overall results from this analysis, we plotted out the AUC receiver operator characteristic (ROC) curves from the combined test set using the eight models with the lowest log-loss scores from the training set (Figure 5F).

## 4 | DISCUSSION

In this study, we used pre-existing neuroimaging biomarker datasets from ADNI to investigate the APOE  $\epsilon$ 4-associated heterogeneity in AD-related pathologies in CN, MCI, and AD participants aged  $\geq 55$  years old. In our diagnostic group-level analyses (Figure 1), while controlling for sex and age, we observed robust APOE  $\epsilon$ 4-associated differences that confirm and further elucidate the known AD-promoting effects of APOE  $\epsilon$ 4. For example, the APOE  $\epsilon$ 4 carriers in this ADNI cohort possessed significantly greater A $\beta$  deposition throughout their brains than the APOE  $\epsilon$ 4 non-carriers in each diagnostic group, which corroborates what is known about APOE  $\epsilon$ 4 increasing A $\beta$  deposition in the brain.<sup>28-35</sup> We also observed increased tau pathology in the APOE  $\epsilon$ 4 carriers from each diagnostic group, which appeared to follow a Braak-like regional pattern<sup>36</sup> with ongoing disease progression, beginning in the entorhinal cortex and the amygdala of CN APOE  $\epsilon$ 4 carriers versus non-carriers, then adding on the hippocampus and the temporal cortex in MCI APOE  $\epsilon$ 4 carriers versus non-carriers, and then adding on regions from the frontal, parietal, and occipital cortices in AD APOE  $\epsilon$ 4 carriers versus non-carriers. We also observed decreased glucose uptake in the MetaROI brain regions of the APOE  $\epsilon$ 4 carriers during this diagnostic group-level analysis, which increases in effect size from CN to MCI to AD APOE  $\epsilon$ 4 carriers versus non-carriers. Furthermore, we observed increased brain atrophy in the APOE  $\epsilon$ 4 carriers versus non-carriers, first in MTL and temporal cortex regions of MCI APOE  $\epsilon$ 4 carriers, and then in the MTL, temporal cortex, and select regions of the frontal (left rostral middle frontal) and parietal (left inferior parietal) cortices of AD APOE  $\epsilon$ 4 carriers. Interestingly, these AD APOE  $\epsilon$ 4 carriers also possessed enlarged inferior lateral ventricles. One exception to this pattern of increasing AD-related pathology in APOE  $\epsilon$ 4 carriers with ongoing disease progression, however, was the TOTAL\_WMh measurements from the FLAIR MRI analysis, which were only observed to be increased in the CN APOE  $\epsilon$ 4 carriers, with no differences observed in the MCI or AD APOE  $\epsilon$ 4 carriers.

There are other valuable observations in these analyses, as well. For example, the sex-stratified results (Figure 2) revealed greater pathological differences in female APOE  $\epsilon$ 4 carriers versus non-carriers, compared to male APOE  $\epsilon$ 4 carriers versus non-carriers. This was true for the A $\beta$  PET results in female CN and MCI participants, the tau

PET results in female CN and MCI participants, the FDG PET results in female MCI participants, and the structural MRI results in female MCI participants. Once again, the only neuroimaging biomarker that did not follow this pattern was the FLAIR MRI results, which showed increased WMH levels in male CN APOE  $\epsilon$ 4 carriers and male MCI APOE  $\epsilon$ 4 carriers, while no differences were observed in female APOE  $\epsilon$ 4 carriers.

In our age stratification analysis (Figure 3), the results were not quite as clear as those obtained from the sex stratification analysis. For example, the 75-and-over CN APOE  $\epsilon$ 4 carriers showed both decreased glucose uptake by FDG PET and increased WMHs by FLAIR MRI, while no changes occurred in the under-75 CN APOE  $\epsilon$ 4 carriers for these two biomarker measures. Meanwhile, the under-75 CN APOE  $\epsilon$ 4 carriers showed decreased CBF levels in several regions, while the 75-and-over CN APOE  $\epsilon$ 4 carriers showed no differences in their CBF levels.

Interestingly, this decreased CBF result in under-75 CN APOE  $\epsilon$ 4 carriers was the only instance in which any regional CBF differences reached significance in APOE  $\epsilon$ 4 carriers versus non-carriers (or in converters vs. non-converters). Overall, the previous results from CBF studies during AD pathogenesis and in APOE  $\epsilon$ 4 carriers have been mixed.<sup>16</sup> Of note, while several studies have reported increased regional CBF levels in younger ( $< 65$  years old) CN APOE  $\epsilon$ 4 carriers,<sup>37-39</sup> there have also been several reports of decreasing CBF levels with age in CN APOE  $\epsilon$ 4 carriers,<sup>38,40,41</sup> which may be reflected in our results. We should point out, however, that the ASL MRI dataset we used for our analysis contained the lowest number of participants of any of the datasets, with this number further reduced in the under-75 analysis (30 APOE  $\epsilon$ 4 carriers, 51 APOE  $\epsilon$ 4 non-carriers). Therefore, larger cohorts should be analyzed to confirm our CBF result.

Finally, we observed several biomarker regions that were significantly different in the CN to MCI/AD converters versus non-converter analysis, in both APOE  $\epsilon$ 4 carriers and in APOE  $\epsilon$ 4 non-carriers (Figure 4). It is very intriguing that five of the six neuroimaging biomarkers showed significant differences between the converters and the non-converters in one or both APOE genotype groups. CN APOE  $\epsilon$ 4 carriers who converted to MCI/AD displayed increased regional levels of A $\beta$ , Tau, and WMHs, while CN APOE  $\epsilon$ 4 non-carriers who converted to MCI/AD displayed increased regional levels of tau and WMHs, as well as increased ventricle size and decreased glucose uptake. This observation suggests that no one pathology dictates progression to MCI/AD, but that several pathological factors are likely involved and perhaps acting in concert during this period of cognitive decline.

We also used this converter analysis to conduct a proof-of-concept machine learning experiment to investigate the possibility that these regional biomarker differences could be used to predict future MCI/AD conversion in cognitively unimpaired individuals (Figure 5). Interestingly, our XGBoosted algorithm identified the MetaROI differences from the FDG PET analysis and the ventricle size differences from the structural MRI as the most important factors in determining CN to MCI/AD conversion, with the FLAIR MRI WMH differences close behind. While it is not possible to determine the exact number of CN to MCI/AD converters needed to confidently perform this analysis, a

general rule of thumb with machine learning experiments is that the ratio of samples to features used to train the model should be at least 10:1 to avoid overfitting (with some machine learning models requiring much larger ratios).<sup>42</sup> Therefore, our current model, which possesses seven features, would require at least 70 converters in the training set alone, with additional converters required if we were to include features from the tau PET and ASL MRI datasets. However, while larger cohorts of APOE  $\epsilon 4$  carrier and non-carrier converters are required, our initial attempt at this approach does suggest that specific combinations of regional biomarker changes may be able to help identify cognitively unimpaired individuals who are likely to convert to MCI or AD in the future.

While the general results from the APOE  $\epsilon 4$  heterogeneity comparisons described above mostly corroborate prior studies, there are some additional nuanced findings that contradict previous reports. In particular, our group previously published a systematic review on the APOE  $\epsilon 4$ -associated cognitive and pathological heterogeneity in patients with AD.<sup>43</sup> Although most of the results in this study correspond to the conclusions we made in that systematic review, there are three conclusions that are not validated by these analyses using the ADNI cohort. Specifically, we reported that in most of the studies we reviewed, patients with AD who were APOE  $\epsilon 4$  carriers did not possess greater levels of A $\beta$  in their brains than APOE  $\epsilon 4$  non-carriers, and that they possessed less tau pathology and larger brain volumes in their frontal and parietal lobes compared to AD APOE  $\epsilon 4$  non-carrier. However, in this ADNI cohort, when controlling for sex and age, AD APOE  $\epsilon 4$  carriers did possess increased A $\beta$  throughout their brains compared to AD APOE  $\epsilon 4$  non-carriers, and they did possess increased tau pathology in their frontal or parietal lobes and decreased brain volumes in one region from both their frontal and parietal lobes compared to AD APOE  $\epsilon 4$  non-carriers.

Finally, while ADNI is an invaluable resource for studies such as ours, it is important to note the limitations associated with the ADNI cohort. First, the ADNI participants from ADNI1/GO/2/3 have relatively high levels of education and are predominantly non-Hispanic White individuals.<sup>44</sup> This lack of ethnic/racial diversity is particularly important, because APOE  $\epsilon 4$  effects are quite variable based on the ethnicity/race of the carrier.<sup>24,26</sup> Second, as mentioned previously, the data generated from these six neuroimaging biomarkers were not obtained from the same ADNI participants (although some overlap does exist). It is important to note, therefore, that the different neuroimaging biomarker results presented in each figure are not directly correlated with one another; we are instead making qualitative comparisons of each biomarker's relative presentation in distinct groups of APOE  $\epsilon 4$  carriers and non-carriers who participated in ADNI. Last, there were often large imbalances and limited sample sizes in some of our groupings that are worth taking note of, as they may reduce the overall power of the statistical comparisons. Most notably, as shown in Table 2, the numbers of CN participants who converted to MCI/AD are relatively small and are significantly smaller than the non-converters.

Even with these limitations, however, we believe that the results presented in this study represent an important step forward in our

understanding of how APOE  $\epsilon 4$  carriers differ from APOE  $\epsilon 4$  non-carriers in their pathological presentation at various stages along the AD continuum. We also think that this study represents an excellent starting point for future investigations that we hope will add additional nuances, as well as mechanistic insights, to the APOE  $\epsilon 4$ -associated heterogeneity in neuroimaging biomarkers reported here. These continued investigations are necessary because understanding disease heterogeneity is vital for the prevention, diagnosis, and treatment of AD.

## ACKNOWLEDGMENTS

This work was supported by grants from the NIA to T.N. (K01 AG061264 and R01 AG070202), as well as a grant from the NIA to L.B.M., V.M., and T.N. (R01 AG078800) and a grant from the NIA to V.M. (R01 AG066831). Data collection and sharing for ADNI is funded by the NIA (U19 AG024904). The grantee organization is the Northern California Institute for Research and Education. In the past, ADNI has also received funding from the National Institute of Biomedical Imaging and Bioengineering, the Canadian Institutes of Health Research, and private sector contributions through the Foundation for the National Institutes of Health (FNIH), including generous contributions from the following: AbbVie; Alzheimer's Association; Alzheimer's Drug Discovery Foundation; Araclon Biotech; BioClinica, Inc.; Biogen; Bristol-Myers Squibb Company; CereSpir, Inc.; Cogstate; Eisai Inc.; Elan Pharmaceuticals, Inc.; Eli Lilly and Company; EuroImmun; F. Hoffmann-La Roche Ltd and its affiliated company Genentech, Inc.; Fujirebio; GE Healthcare; IXICO Ltd.; Janssen Alzheimer Immunotherapy Research & Development, LLC; Johnson & Johnson Pharmaceutical Research & Development LLC; Lumosity; Lundbeck; Merck & Co., Inc.; Meso Scale Diagnostics, LL.; NeuroRx Research; Neurotrack Technologies; Novartis Pharmaceuticals Corporation; Pfizer Inc.; Piramal Imaging; Servier; Takeda Pharmaceutical Company; and Transition Therapeutics.

## CONFLICT OF INTEREST STATEMENT

Tal Nuriel is a consultant for Mubadala Capital. The other authors declare no conflicts of interest. Author disclosures are available in the [supporting information](#).

## CONSENT STATEMENT

No consent was required, as all human subject data were collected by ADNI investigators and were provided as de-identified datasets downloaded from the ADNI website. Furthermore, all data were used in accordance with ADNI's Data Use Agreement.

## ORCID

Tal Nuriel  <https://orcid.org/0000-0002-5252-8048>

## REFERENCES

1. Alzheimer A, Stelzmann RA, Schnitzlein HN, Murtagh FR. An English translation of Alzheimer's 1907 paper, "Über eine eigenartige Erkrankung der Hirnrinde". *Clin Anat*. 1995;8:429-431.
2. Jack CR Jr, Bennett DA, Blennow K, et al. A/T/N: an unbiased descriptive classification scheme for Alzheimer disease biomarkers. *Neurology*. 2016;87:539-547.

3. Reiman EM, Chen K, Alexander GE, et al. Functional brain abnormalities in young adults at genetic risk for late-onset Alzheimer's dementia. *Proc Natl Acad Sci USA*. 2004;101:284-289.
4. Reiman EM, Caselli RJ, Yun LS, et al. Preclinical evidence of Alzheimer's disease in persons homozygous for the epsilon 4 allele for apolipoprotein E. *N Engl J Med*. 1996;334:752-758.
5. Reiman EM, Caselli RJ, Chen K, Alexander GE, Bandy D, Frost J. Declining brain activity in cognitively normal apolipoprotein E epsilon 4 heterozygotes: a foundation for using positron emission tomography to efficiently test treatments to prevent Alzheimer's disease. *Proc Natl Acad Sci USA*. 2001;98:3334-3339.
6. Menon V. 20 years of the default mode network: a review and synthesis. *Neuron*. 2023;111:2469-2487.
7. Hamalainen A, Pihlajamaki M, Tanila H, et al. Increased fMRI responses during encoding in mild cognitive impairment. *Neurobiol Aging*. 2007;28:1889-1903.
8. Kircher TT, Weis S, Freymann K, et al. Hippocampal activation in patients with mild cognitive impairment is necessary for successful memory encoding. *J Neurol Neurosurg Psychiatry*. 2007;78:812-818.
9. Bakker A, Krauss GL, Albert MS, et al. Reduction of hippocampal hyperactivity improves cognition in amnesic mild cognitive impairment. *Neuron*. 2012;74:467-474.
10. Dickerson BC, Salat DH, Greve DN, et al. Increased hippocampal activation in mild cognitive impairment compared to normal aging and AD. *Neurology*. 2005;65:404-411.
11. Miller SL, Fenstermacher E, Bates J, Blacker D, Sperling RA, Dickerson BC. Hippocampal activation in adults with mild cognitive impairment predicts subsequent cognitive decline. *J Neurol Neurosurg Psychiatry*. 2008;79:630-635.
12. Quiroz YT, Budson AE, Celone K, et al. Hippocampal hyperactivation in presymptomatic familial Alzheimer's disease. *Ann Neurol*. 2010;68:865-873.
13. Sepulveda-Falla D, Glatzel M, Lopera F. Phenotypic profile of early-onset familial Alzheimer's disease caused by presenilin-1 E280A mutation. *J Alzheimers Dis*. 2012;32:1-12.
14. Filippini N, MacIntosh BJ, Hough MG, et al. Distinct patterns of brain activity in young carriers of the APOE-epsilon4 allele. *Proc Natl Acad Sci USA*. 2009;106:7209-7214.
15. Suri S, Mackay CE, Kelly ME, et al. Reduced cerebrovascular reactivity in young adults carrying the APOE epsilon4 allele. *Alzheimers Dement*. 2015;11:648-657 e1.
16. Zhang N, Gordon ML, Goldberg TE. Cerebral blood flow measured by arterial spin labeling MRI at resting state in normal aging and Alzheimer's disease. *Neurosci Biobehav Rev*. 2017;72:168-175.
17. Desmarais P, Gao AF, Lancot K, et al. White matter hyperintensities in autopsy-confirmed frontotemporal lobar degeneration and Alzheimer's disease. *Alzheimers Res Ther*. 2021;13:129.
18. Garnier-Crussard A, Bougacha S, Wirth M, et al. White matter hyperintensity topography in Alzheimer's disease and links to cognition. *ion*. 2022;18:422-433.
19. Yoshita M, Fletcher E, Harvey D, et al. Extent and distribution of white matter hyperintensities in normal aging, MCI, and AD. *Neurology*. 2006;67:2192-2198.
20. Wardlaw JM, Smith EE, Biessels GJ, et al. Neuroimaging standards for research into small vessel disease and its contribution to ageing and neurodegeneration. *Lancet Neurol*. 2013;12:822-838.
21. Garnier-Crussard A, Cotton F, Krolak-Salmon P, Chetelat G. White matter hyperintensities in Alzheimer's disease: beyond vascular contribution. *Alzheimers Dement*. 2023;19:3738-3748.
22. Austin PC, Leckie G. The effect of number of clusters and cluster size on statistical power and Type I error rates when testing random effects variance components in multilevel linear and logistic regression models. *J Stat Comput Simul*. 2018;88:3151-3163.
23. Bell BA, Ferron JM, Kromrey JD. Cluster size in multilevel models: the impact of sparse data structures on point and interval estimates in two-level models. In: *JSM Proceedings, Survey Research Methods Section*. American Statistical Association; 2008:1122-1129.
24. Farrer LA, Cupples LA, Haines JL, et al. Effects of age, sex, and ethnicity on the association between apolipoprotein E genotype and Alzheimer disease. A meta-analysis. APOE and Alzheimer Disease Meta Analysis Consortium. *JAMA*. 1997;278:1349-1356.
25. Altmann A, Tian L, Henderson VW, Greicius MD. Alzheimer's Disease Neuroimaging Initiative I. Sex modifies the APOE-related risk of developing Alzheimer disease. *Ann Neurol*. 2014;75:563-573.
26. Belloy ME, Andrews SJ, Le Guen Y, et al. APOE genotype and Alzheimer disease risk across age, sex, and population ancestry. *JAMA Neurol*. 2023;80:1284-1294.
27. Schneider P, Khafa F. Chapter 8 - Machine learning: ML for eHealth systems. In: Schneider P, Khafa F, eds. *Anomaly Detection and Complex Event Processing over IoT Data Streams*. Academic Press; 2022:149-191.
28. Bales KR, Verina T, Dodel RC, et al. Lack of apolipoprotein E dramatically reduces amyloid beta-peptide deposition. *Nat Genet*. 1997;17:263-264.
29. Castano EM, Prelli F, Wisniewski T, et al. Fibrillogenesis in Alzheimer's disease of amyloid beta peptides and apolipoprotein E. *Biochem J*. 1995;306(Pt 2):599-604.
30. Rebeck GW, Reiter JS, Strickland DK, Hyman BT. Apolipoprotein E in sporadic Alzheimer's disease: allelic variation and receptor interactions. *Neuron*. 1993;11:575-580.
31. Schmechel DE, Saunders AM, Strittmatter WJ, et al. Increased amyloid beta-peptide deposition in cerebral cortex as a consequence of apolipoprotein E genotype in late-onset Alzheimer disease. *Proc Natl Acad Sci USA*. 1993;90:9649-9653.
32. Ma J, Yee A, Brewer HB Jr, Das S, Potter H. Amyloid-associated proteins alpha 1-antichymotrypsin and apolipoprotein E promote assembly of Alzheimer beta-protein into filaments. *Nature*. 1994;372:92-94.
33. Castellano JM, Kim J, Stewart FR, et al. Human apoE isoforms differentially regulate brain amyloid-beta peptide clearance. *Sci Transl Med*. 2011;3:89ra57.
34. Holtzman DM, Bales KR, Tenkova T, et al. Apolipoprotein E isoform-dependent amyloid deposition and neuritic degeneration in a mouse model of Alzheimer's disease. *Proc Natl Acad Sci USA*. 2000;97:2892-2897.
35. Reiman EM, Chen K, Liu X, et al. Fibrillar amyloid-beta burden in cognitively normal people at 3 levels of genetic risk for Alzheimer's disease. *Proc Natl Acad Sci USA*. 2009;106:6820-6825.
36. Braak H, Alafuzoff I, Arzberger T, Kretzschmar H, Del Tredici K. Staging of Alzheimer disease-associated neurofibrillary pathology using paraffin sections and immunocytochemistry. *Acta Neuropathol*. 2006;112:389-404.
37. Dounavi ME, Mak E, Swann P, et al. Differential association of cerebral blood flow and anisocytosis in APOE epsilon4 carriers at midlife. *J Cereb Blood Flow Metab*. 2023;43:1672-1684.
38. Wierenga CE, Clark LR, Dev SI, et al. Interaction of age and APOE genotype on cerebral blood flow at rest. *J Alzheimers Dis*. 2013;34:921-935.
39. Fleisher AS, Podraza KM, Bangen KJ, et al. Cerebral perfusion and oxygenation differences in Alzheimer's disease risk. *Neurobiol Aging*. 2009;30:1737-1748.
40. Thambisetty M, Beason-Held L, An Y, Kraut MA, Resnick SM. APOE epsilon4 genotype and longitudinal changes in cerebral blood flow in normal aging. *Arch Neurol*. 2010;67:93-98.
41. Filippini N, Ebmeier KP, MacIntosh BJ, et al. Differential effects of the APOE genotype on brain function across the lifespan. *Neuroimage*. 2011;54:602-610.
42. Alwosheel A, van Cranenburgh S, Chorus CG. Is your dataset big enough? Sample size requirements when using artificial neural networks for discrete choice analysis. *J Choice Model*. 2018;28:167-182.
43. Emrani S, Arain HA, DeMarshall C, Nuriel T. APOE4 is associated with cognitive and pathological heterogeneity in patients with Alzheimer's disease: a systematic review. *Alzheimers Res Ther*. 2020;12:141.

44. Petersen RC, Aisen PS, Beckett LA, et al. Alzheimer's Disease Neuroimaging Initiative (ADNI): clinical characterization. *Neurology*. 2010;74:201-209.

#### SUPPORTING INFORMATION

Additional supporting information can be found online in the Supporting Information section at the end of this article.

**How to cite this article:** Mares J, Kumar G, Sharma A, et al.; for the Alzheimer's Disease Neuroimaging Initiative. APOE  $\epsilon$ 4-associated heterogeneity of neuroimaging biomarkers across the Alzheimer's disease continuum. *Alzheimer's Dement*. 2025;21:e14392. <https://doi.org/10.1002/alz.14392>